Supplementary data for the article:

Steen, J. D.; Stepanovic, S.; Parvizian, M.; De Boer, J. W.; Hage, R.; Chen, J.; Swart, M.; Gruden, M.; Browne, W. R. Lewis versus Brønsted Acid Activation of a Mn(IV) Catalyst for Alkene Oxidation. *Inorganic Chemistry* **2019**, *58* (21), 14924–14930. https://doi.org/10.1021/acs.inorgchem.9b02737

Supporting Information

Lewis vs Brønsted Acid Activation of a Mn(IV) Catalyst for Alkene Oxidation

Jorn D. Steen, Stepan Stepanovic, Mahsa Parvizian, Johannes W. de Boer, Ronald Hage, Juan Chen, Marcel Swart, Maja Gruden,* Wesley R. Browne*

Table of Contents

Additional spectroscopic and voltammetric data

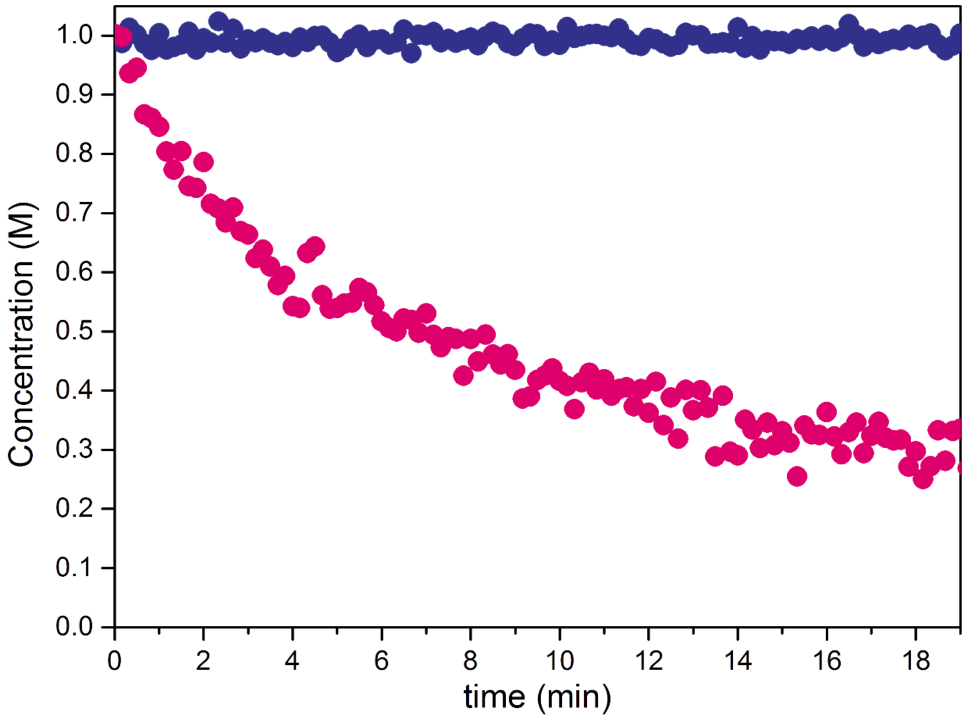

Figure S1 Consumption of H_2O_2 (magenta) with no observable styrene (blue) conversion by **1** (1 mM) in CH_3CN.

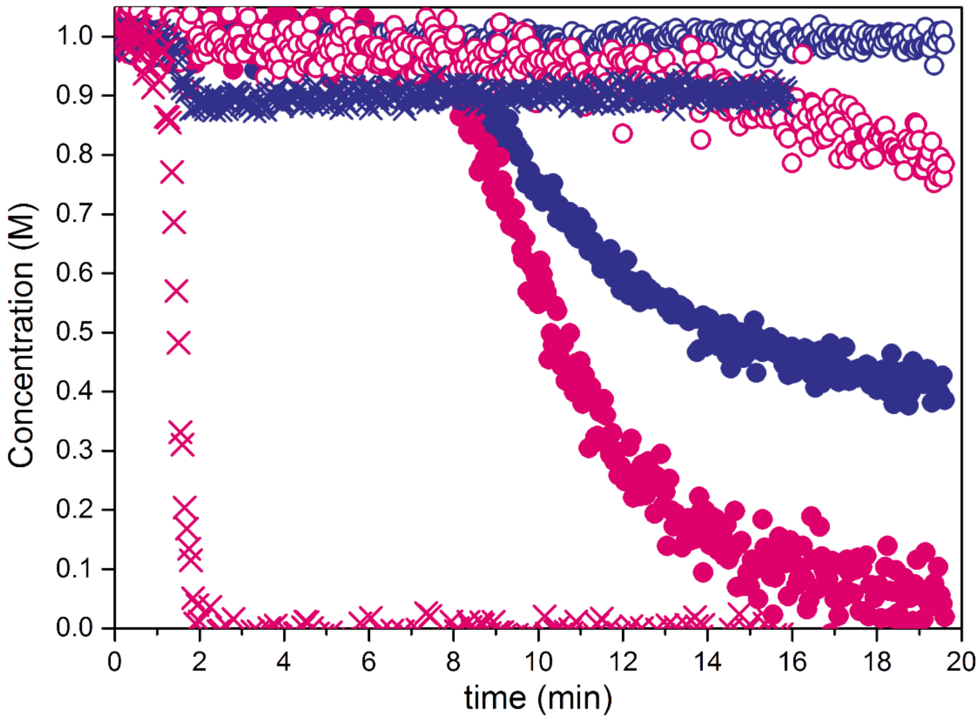

Figure S2 Comparison of kinetics of styrene conversion (blue) and H_2O_2 consumption (magenta) by **1** (1 mM) activated by either $Al(OTf)_3$ (2 eq.; filled), $Y(OTf)_3$ (2 eq.; empty), or $Y(CF_3CO_2)_3$ (2 eq.; cross) for a 17 h standing time.

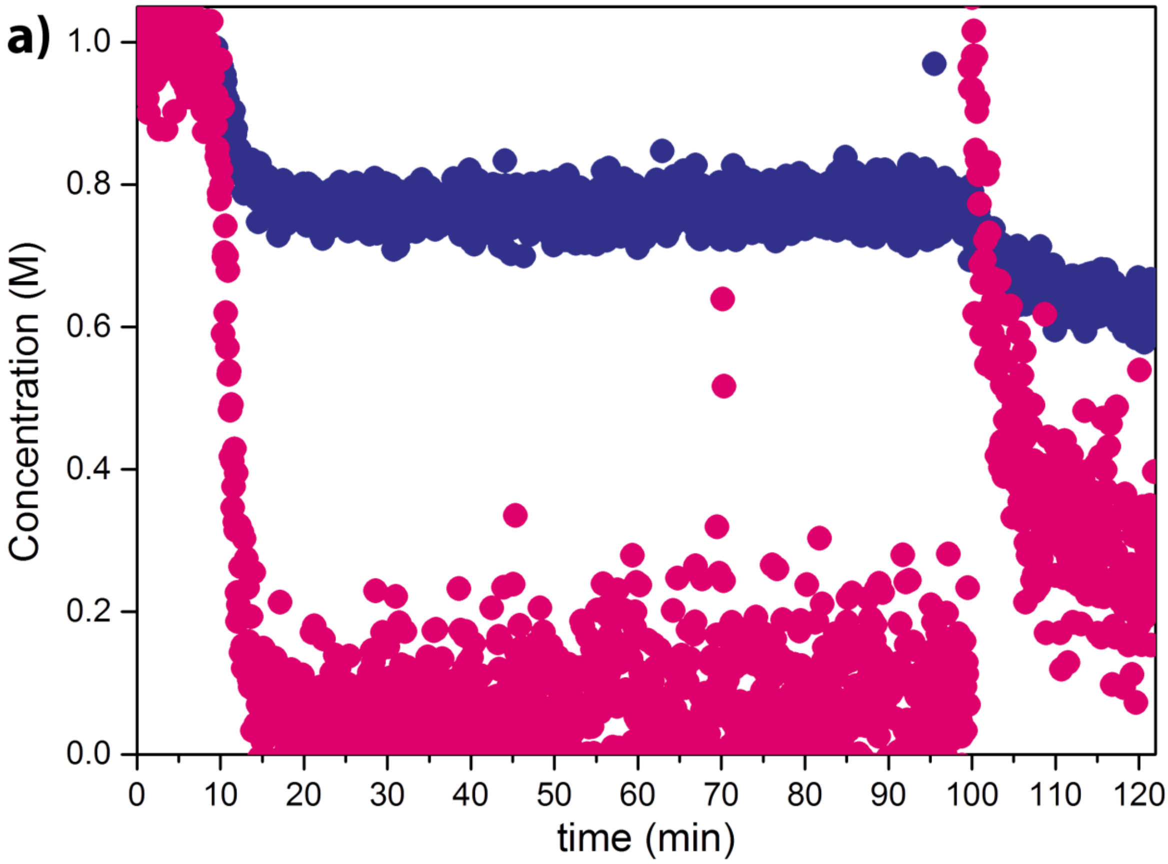

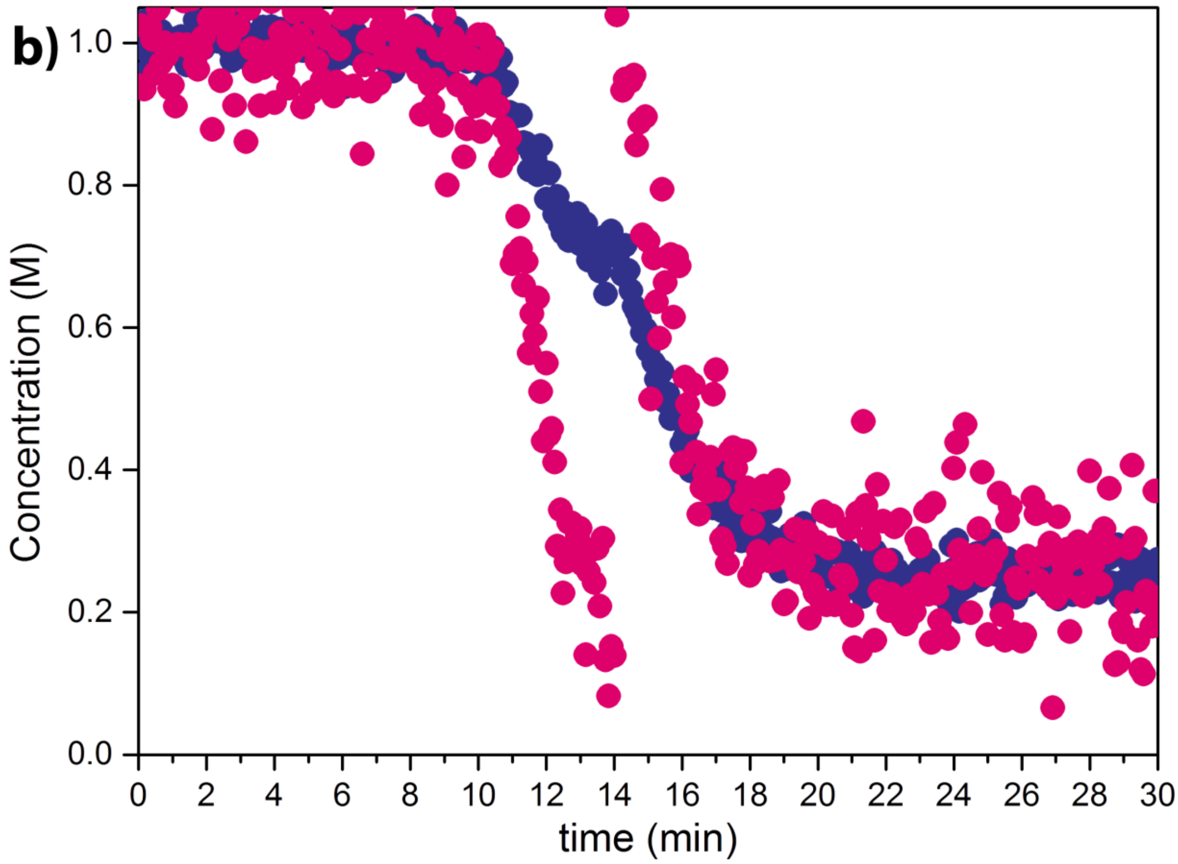

Figure S3 Comparison of H_2O_2 consumption (magenta) and styrene conversion (blue) catalyzed by **1** (1 mM) upon activation by (a) $Sc(OTf)_3$ (2 mM) or (b) TfOH (6 mM) after the addition of a second equivalent of H_2O_2 at t = 100 min or t = 14 min, respectively. Standing time was 1 h.

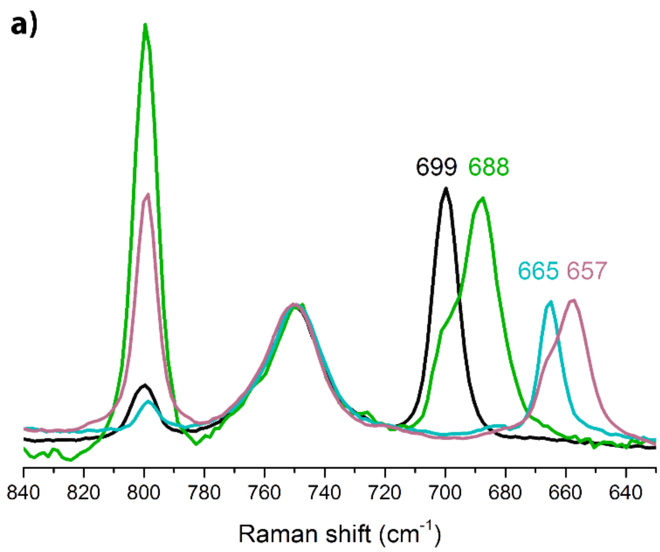

b)	Experimental	Calculated
^{16}O-**1**	699	707
^{18}O-**1**	665	672
Δ[^{18}O] of **1**	34	35
^{16}O-H**1**$^{+}$	688	691
^{18}O-H**1**$^{+}$	657	660
Δ[^{18}O] of H**1**$^{+}$	31	31
Δ[H^{+}] ^{16}O-**1**	11	16
Δ[H^{+}] ^{18}O-**1**	8	12

Figure S4 (a) Experimental Raman spectra (λ_{exc} 355 nm) of **1** before (black) and after addition of $Sc(OTf)_3$ (3 eq.; green) and of ^{18}O-**1** before (cyan) and after addition of $Sc(OTf)_3$ (3 eq.; pink). (b) Comparison of experimental and calculated Raman shifts of **1** and ^{18}O-**1** with and without protonation.

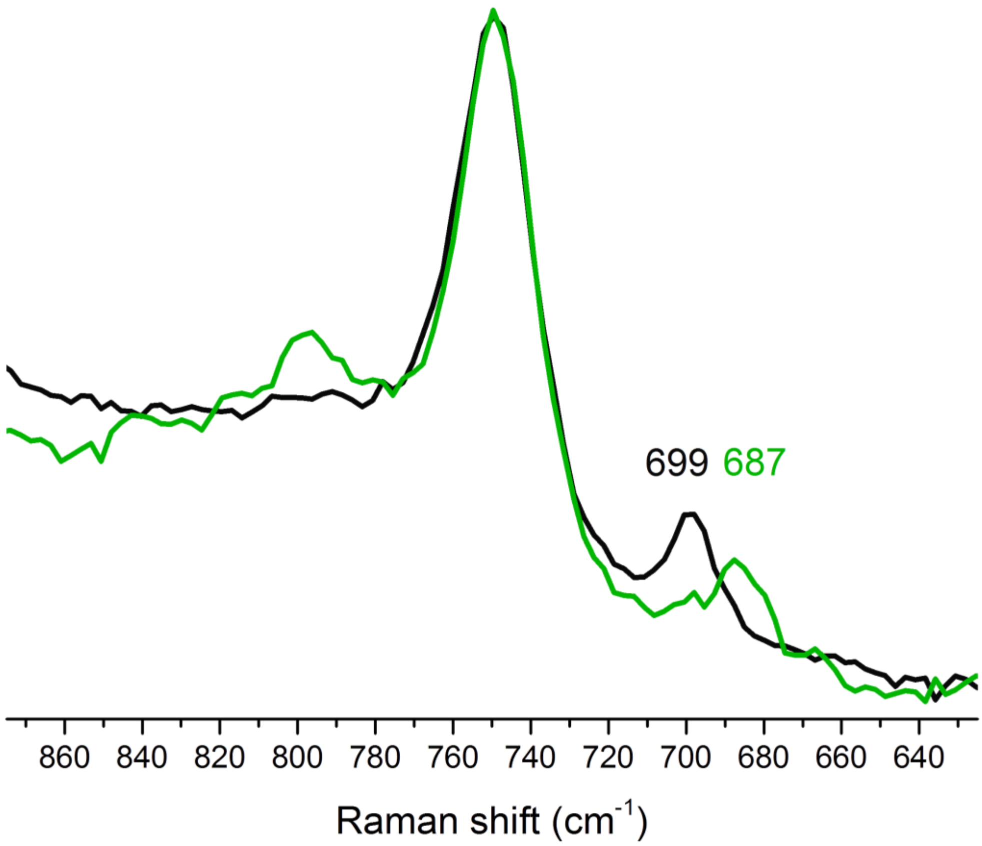

Figure S5 Raman spectrum (λ_{exc} 457 nm) of **1** before (gray) and after (green) addition of $Sc(OTf)_3$ (2 eq.)

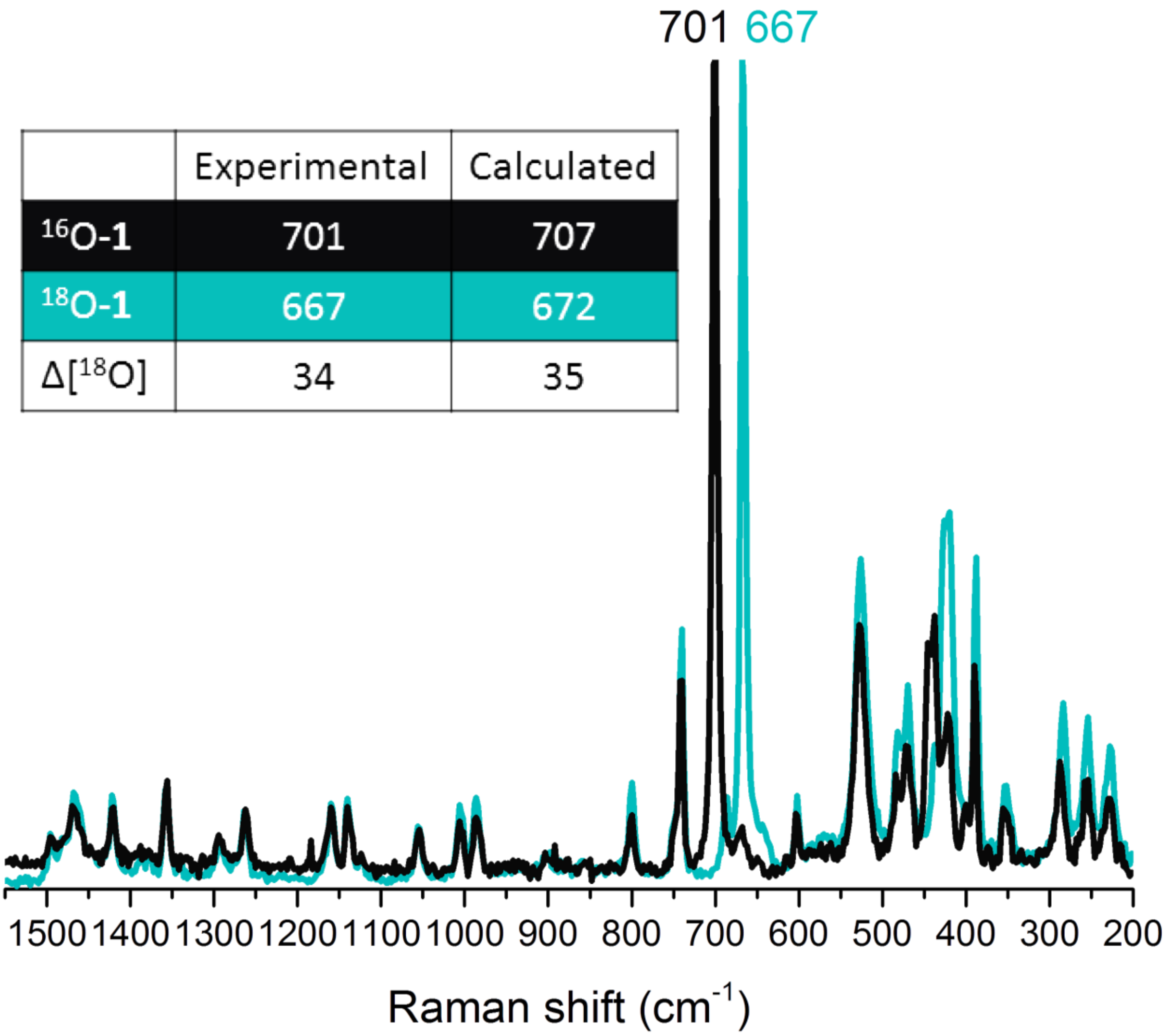

	Experimental	Calculated
^{16}O-1	701	707
^{18}O-1	667	672
Δ[^{18}O]	34	35

Figure S6 Comparison of solid state Raman spectra (λ_{exc} 785 nm) of **1** (black) and ^{18}O-**1** (cyan). In the table the Δ[^{18}O] are depicted for both the experimental and the calculated symmetric Mn-O-Mn vibrational modes, which are in good agreement. There is a minor contribution from incompletely isotopically labelled **1** present in the sample manifested in the weak band at 687 cm^{-1}.

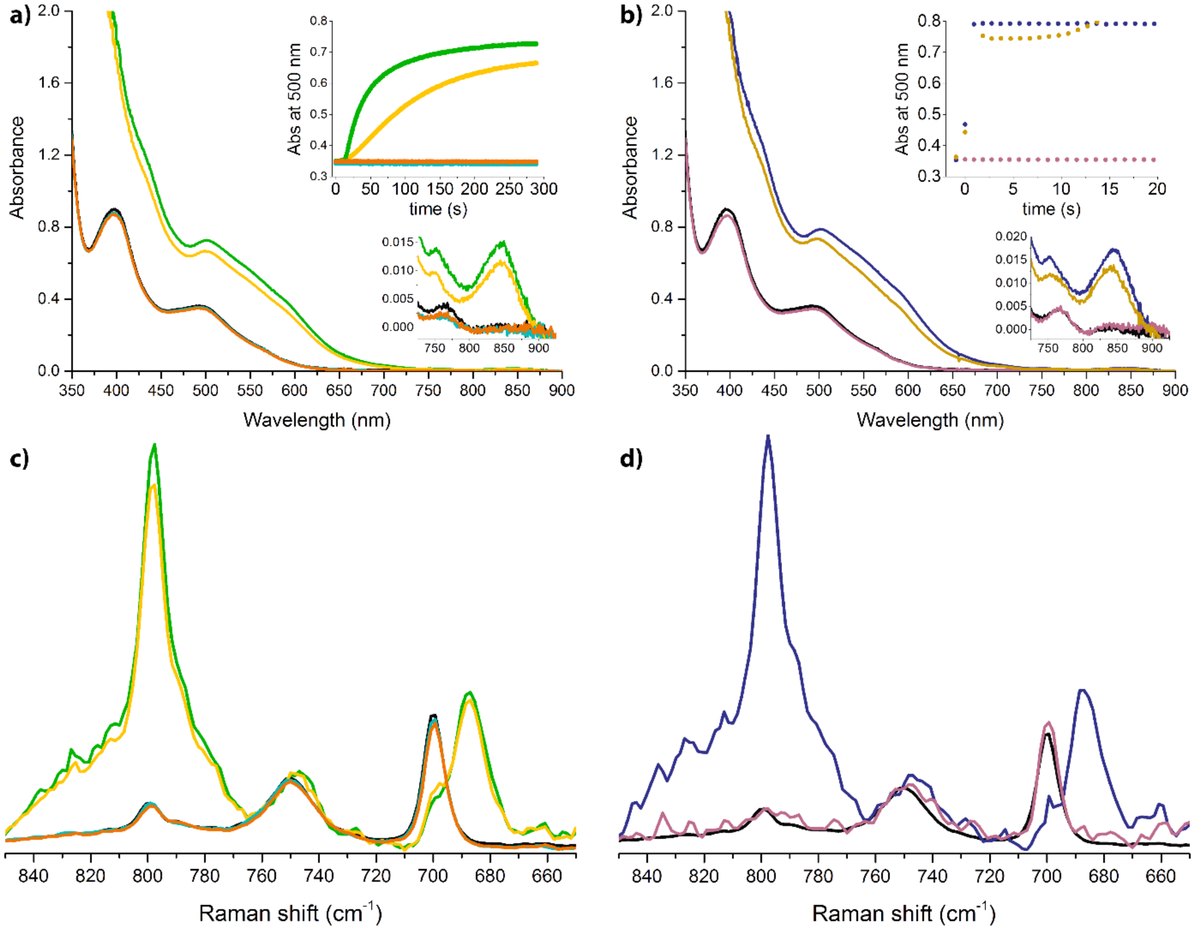

Figure S7 (a) UV/Vis absorption spectroscopy of **1** in CH_3CN before (black) and after addition of $Sc(OTf)_3$ (2 eq.; green), $Al(OTf)_3$ (2 eq.; yellow), $Y(OTf)_3$ (2 eq.; cyan), or $Y(CF_3CO_2)_3$ (2 eq.; orange) with the inset showing the increase in absorbance of the band at 500 nm for the addition of each Lewis acid triflate. (b) UV/Vis absorption spectroscopy of **1** in CH_3CN before (black) and after addition of TfOH (6 eq.; blue), CF_3CO_2H (6 eq.; pink), or H_2SO_4 (240 eq.; gold) with the inset showing the increase in absorbance of the band at 500 nm for the addition of each Brønsted acid. After the addition of H_2SO_4 a red solid precipitates, most likely the sulfate salt of **1**, which causes an increase in absorbance at 500 nm due to scattering after approximately 10 s. (c) Raman spectra (λ_{exc} 355 nm) of **1** in CH_3CN before (black) and after addition of $Sc(OTf)_3$ (2 eq.; green), $Al(OTf)_3$ (2 eq.; yellow), $Y(OTf)_3$ (2 eq.; cyan), or $Y(CF_3CO_2)_3$ (2 eq.; orange). (d) Raman spectra (λ_{exc} 355 nm) of **1** in CH_3CN before (black) and after addition of TfOH (6 eq.; blue), or CF_3CO_2H (6 eq.; pink). For a Raman spectrum of **1** after the addition of H_2SO_4 see Figure S155.

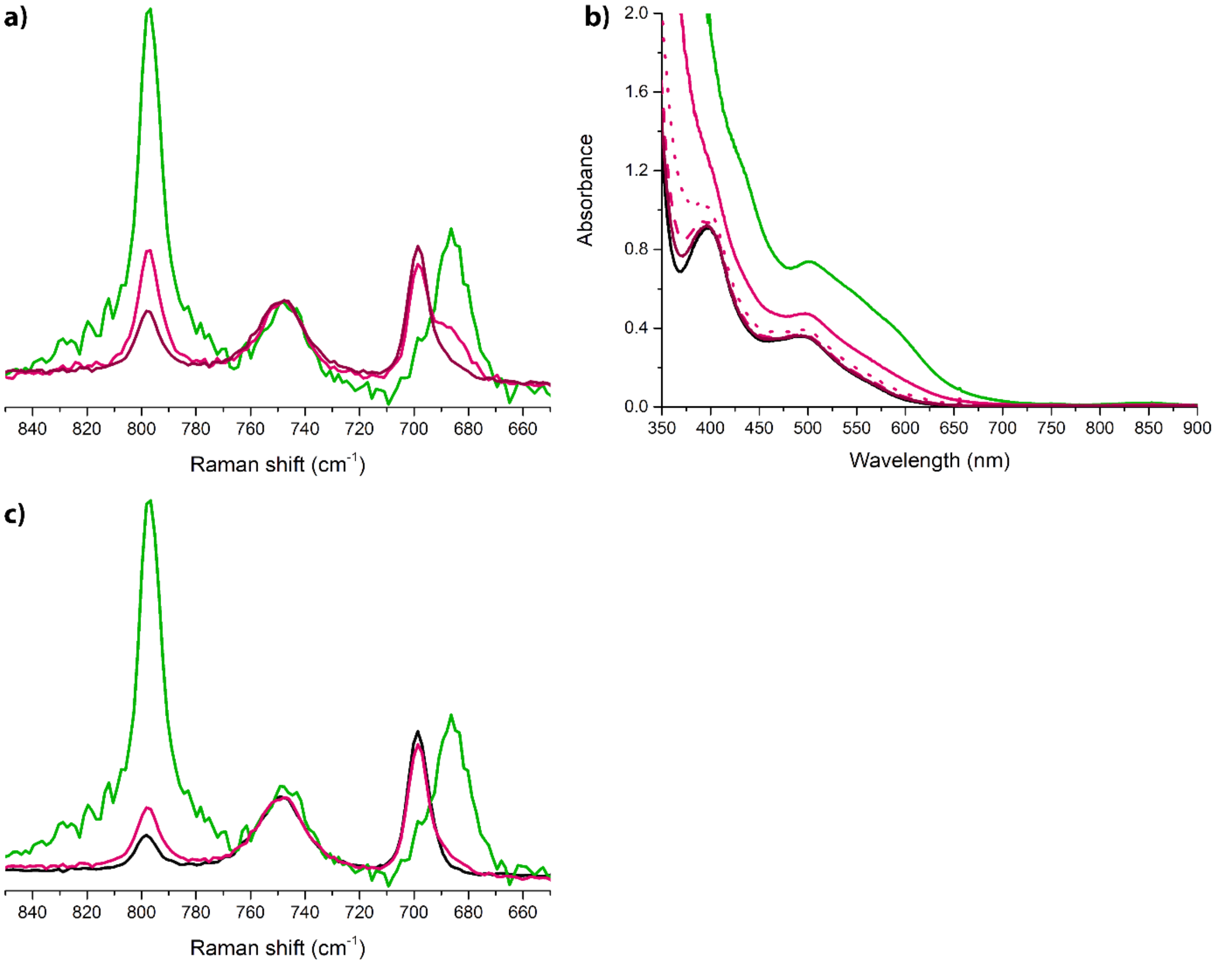

Figure S8 (a) Raman spectra (λ_{exc} 355 nm) of **1** in CH_3CN after addition of $Sc(OTf)_3$ (2 eq.; green) and after subsequent additions of 2 µl (magenta) and 4 µl (dark magenta) of water. Total volume 1.5 ml. (b) UV/Vis absorption spectroscopy of **1** (black) in CH_3CN after addition of $Sc(OTf)_3$ (2 eq.; green) and after subsequent additions of 2 µl (magenta solid), 4 µl (magenta dotted), 6 µl (magenta dashed), and 8 µl (dark magenta) of water. Total volume 1.5 ml. (c) Raman spectra (λ_{exc} 355 nm) of **1** in CH_3CN before (black) and after addition of $Sc(OTf)_3$ (2 eq.; green) and subsequently $H_2{}^{18}O$ (147 eq.; magenta).

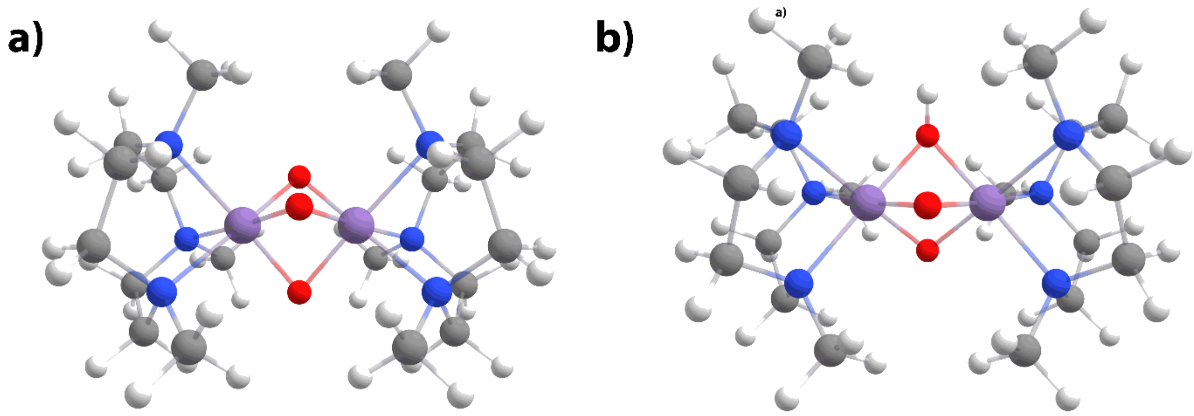

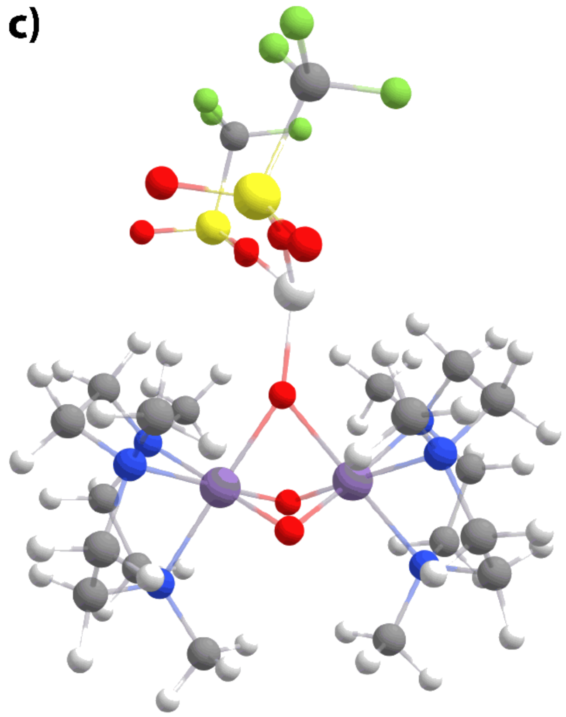

d) Vibrational mode	1	H1+	Sc(OTf)$_2$-1
Symmetrical Mn-O-Mn (Raman active)	707	691	703
Asymmetrical Mn-O-Mn (IR active)	671	661	657

Figure S9 Calculated structures of (a) **1**, (b) H**1**$^+$, and (c) Sc(OTf)$_2$-**1**, with (d) the frequencies in cm^{-1} of the corresponding symmetrical and asymmetrical Mn-O-Mn vibrational modes of each structure.

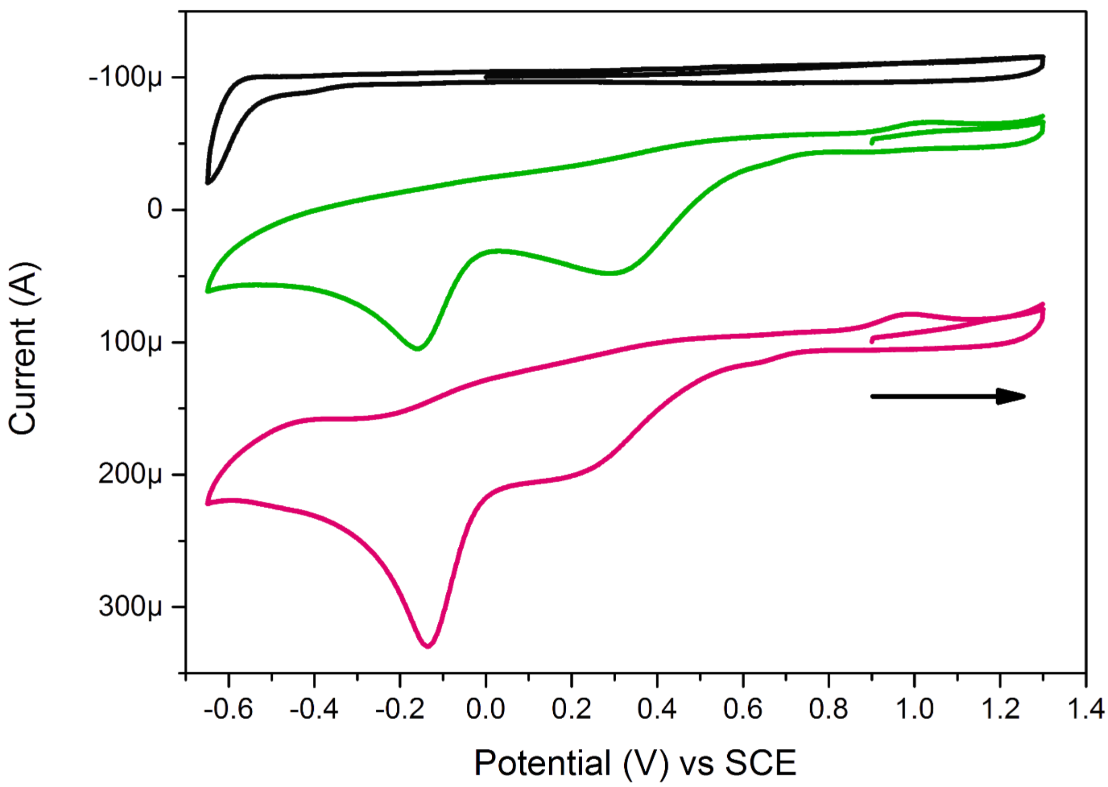

Figure S10 Cyclic voltammograms of **1** (black) in 0.1 M $TBAPF_6$ in CH_3CN after addition of $Sc(OTf)_3$ (3 eq.; green) and after subsequent addition of H_2O (110 eq.; magenta).

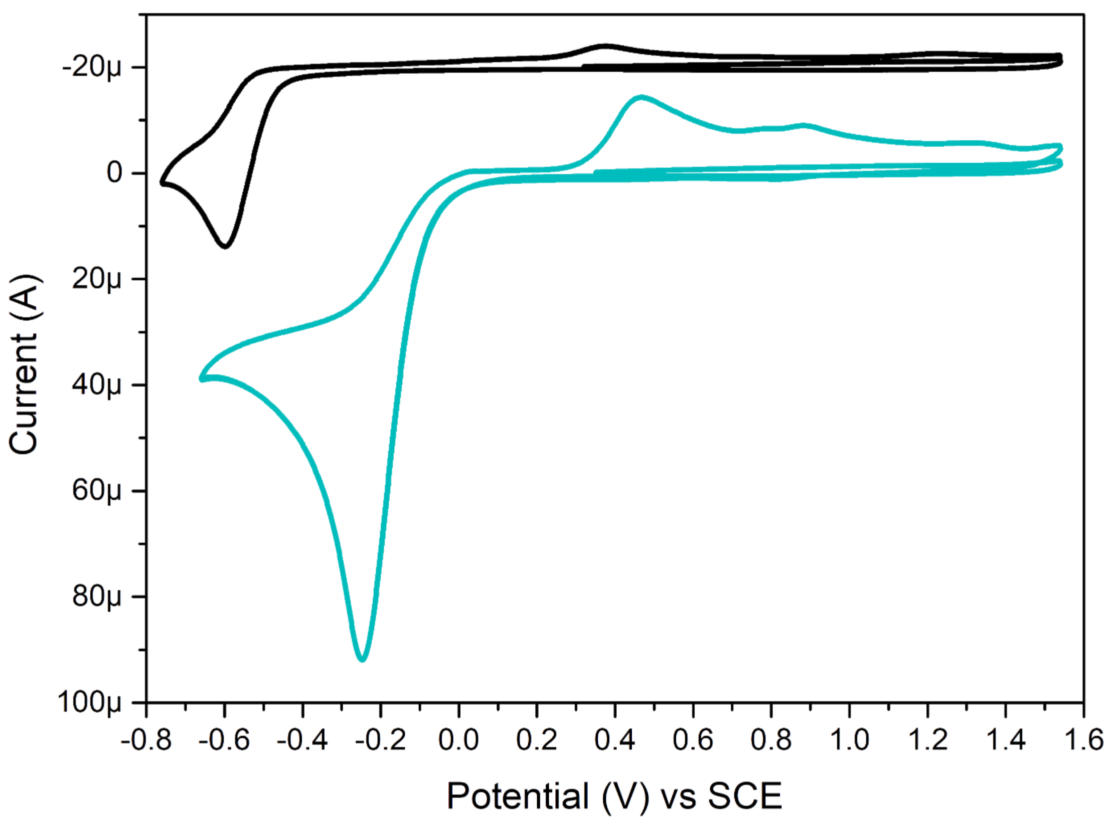

Figure S11 Cyclic voltammograms of **1** without (black) and with (cyan) excess CH_3CO_2H in 0.1 M $TBAPF_6$ in CH_3CN.

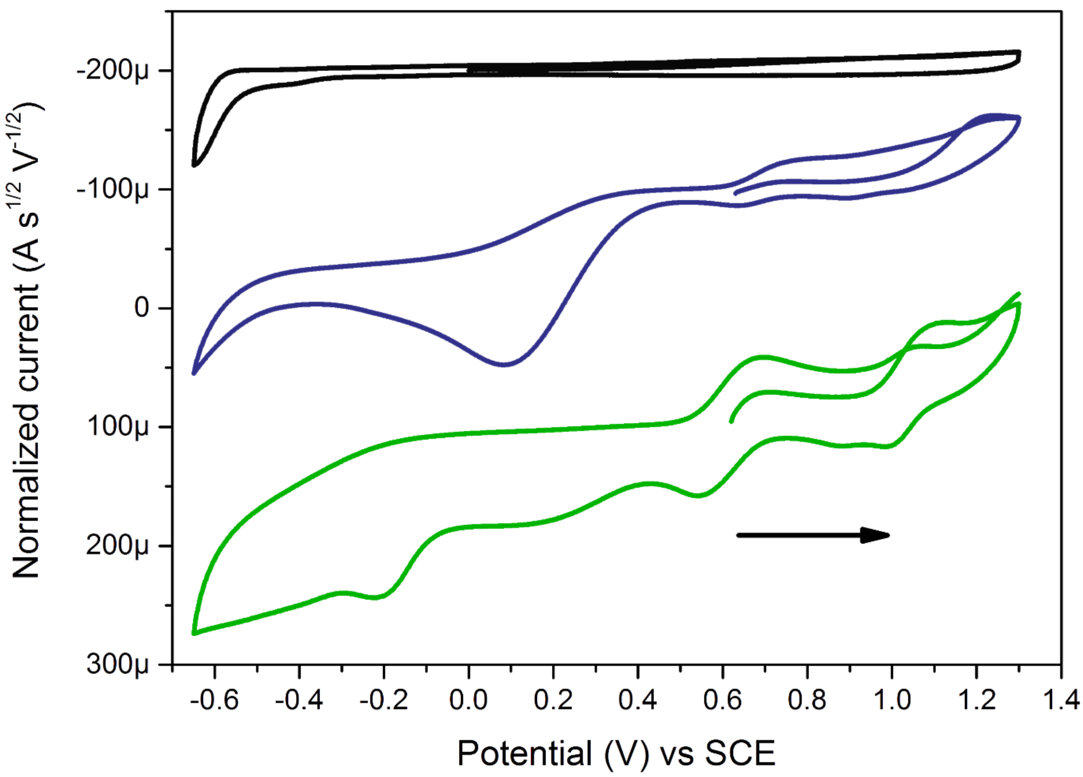

Figure S12 Cyclic voltammograms of **1** (black) after the addition of water and waiting for approximately 30 min after the addition of either TfOH (9 eq.; blue) or $Sc(OTf)_3$ (3 eq.; green). In both cases a species forms with a redox potential of around 0.60 V vs SCE.

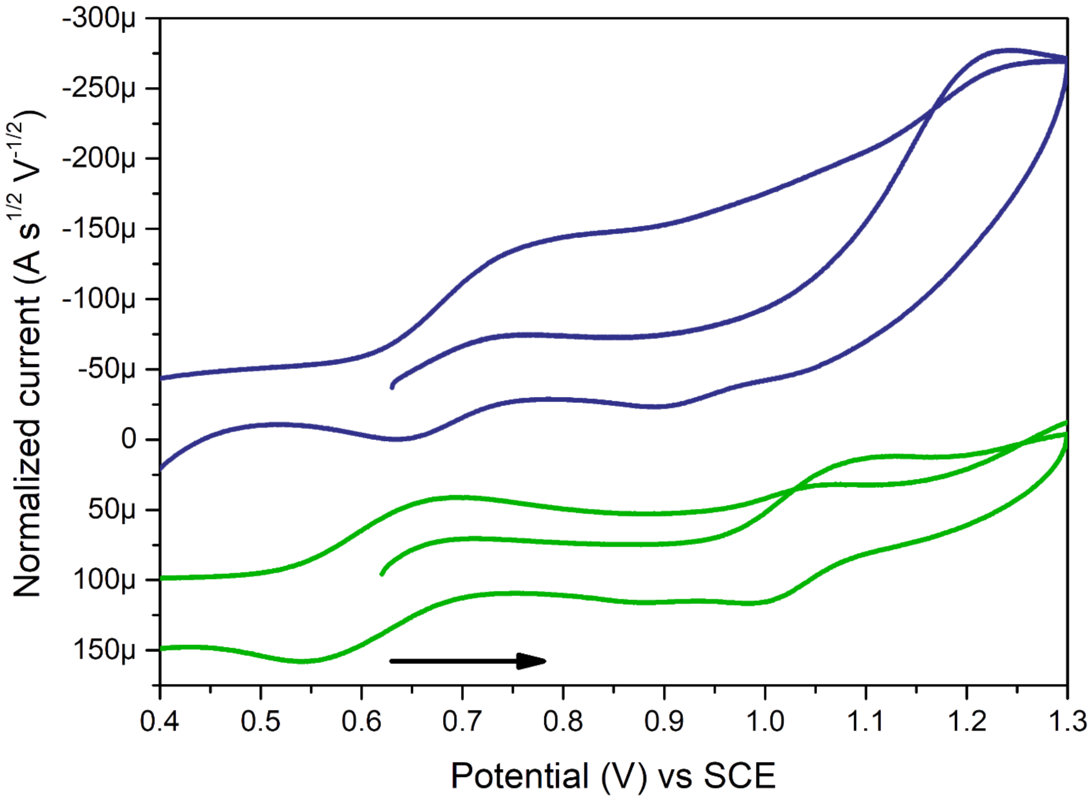

Figure S13 Expansion of CVs of **1** (from Figure S12) with TfOH (9 eq.; blue) and $Sc(OTf)_3$ (3 eq.; green) after the addition of water and waiting for approximately 30 min after the addition (multiplied by a factor for comparison).

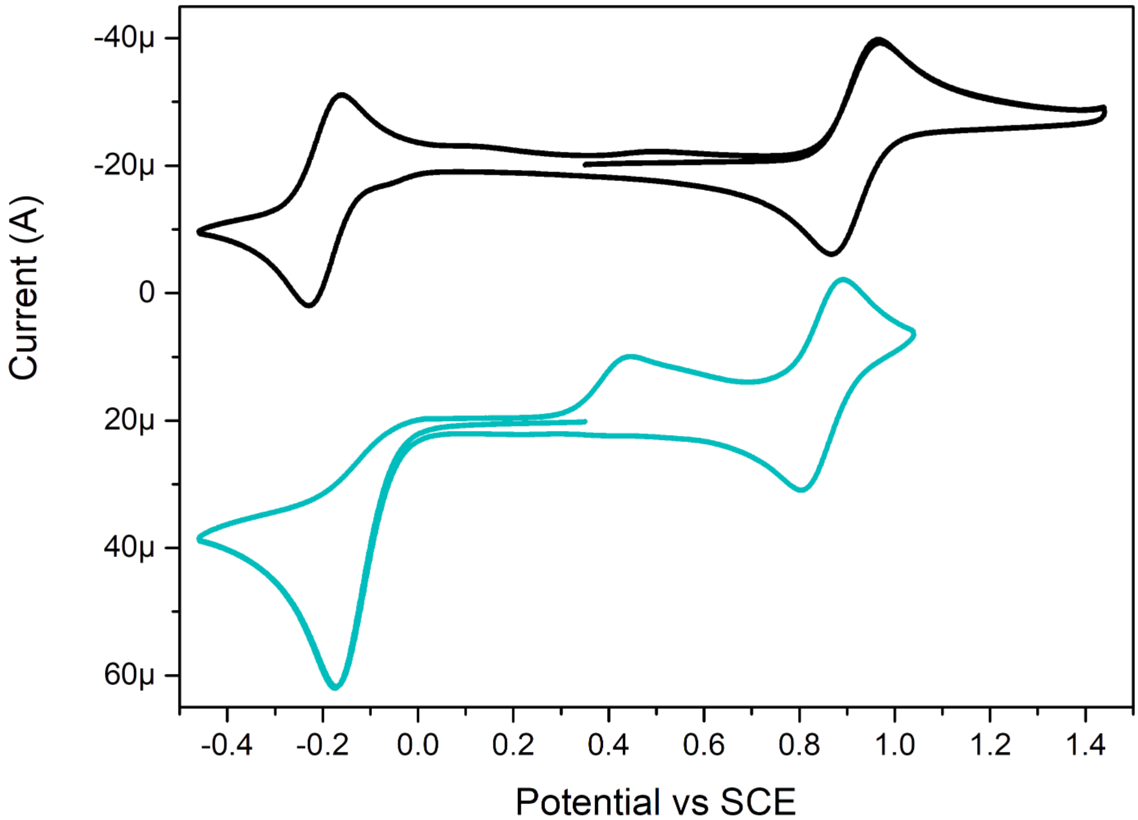

Figure S14 Cyclic voltammograms of $[Mn^{III}_2(\mu\text{-}O)(\mu\text{-}OAc)_2(tmtacn)_2]^{2+}$ (1 mM) without (black) and with (cyan) excess CH_3CO_2H in 0.1 M $TBAPF_6$ in CH_3CN.

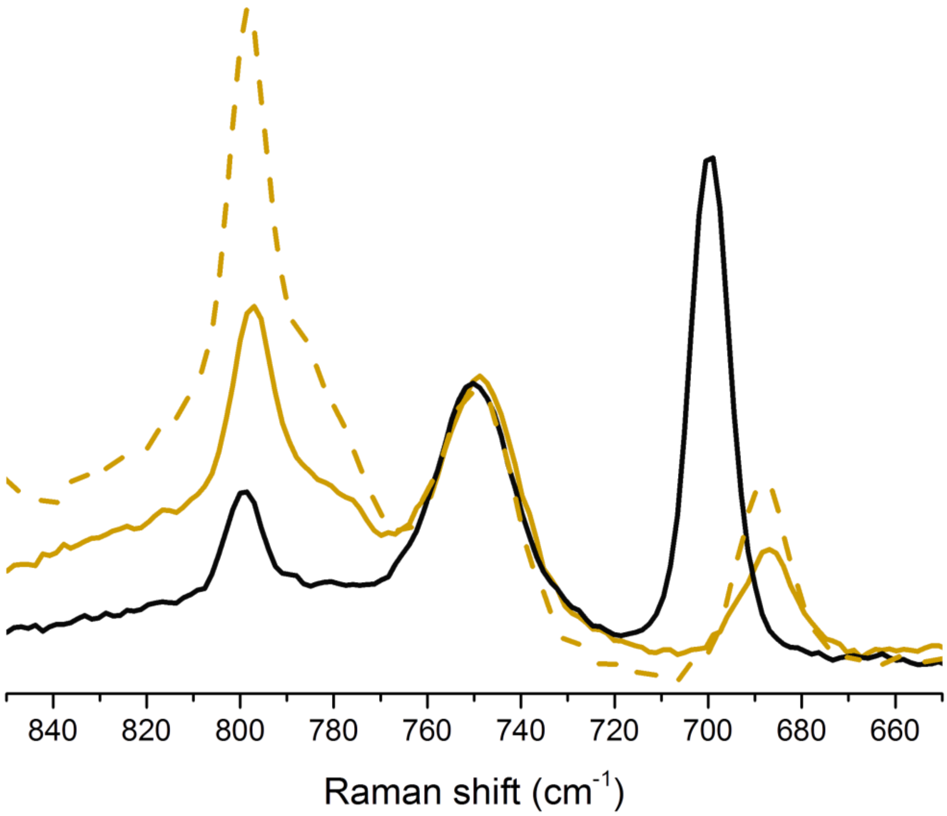

Figure S15 Raman spectra (λ_{exc} 355 nm) of **1** in CH_3CN before (black) and after addition of H_2SO_4 (480 eq.; gold, solid) or D_2SO_4 (480 eq.; gold, dashed).

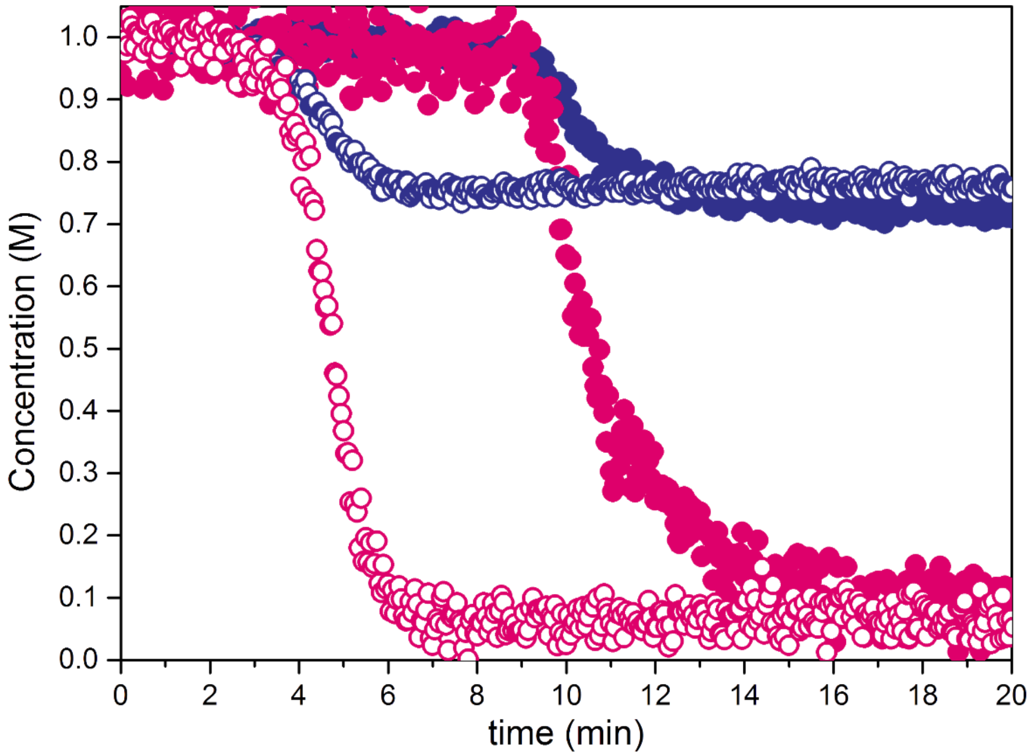

Figure S16 Comparison of kinetics of styrene conversion (blue) and H_2O_2 consumption (magenta) by **1** (1 mM) activated by either TfOH (6 eq.; filled) or CF_3CO_2H (6 eq.; empty) for a 10 min standing time.

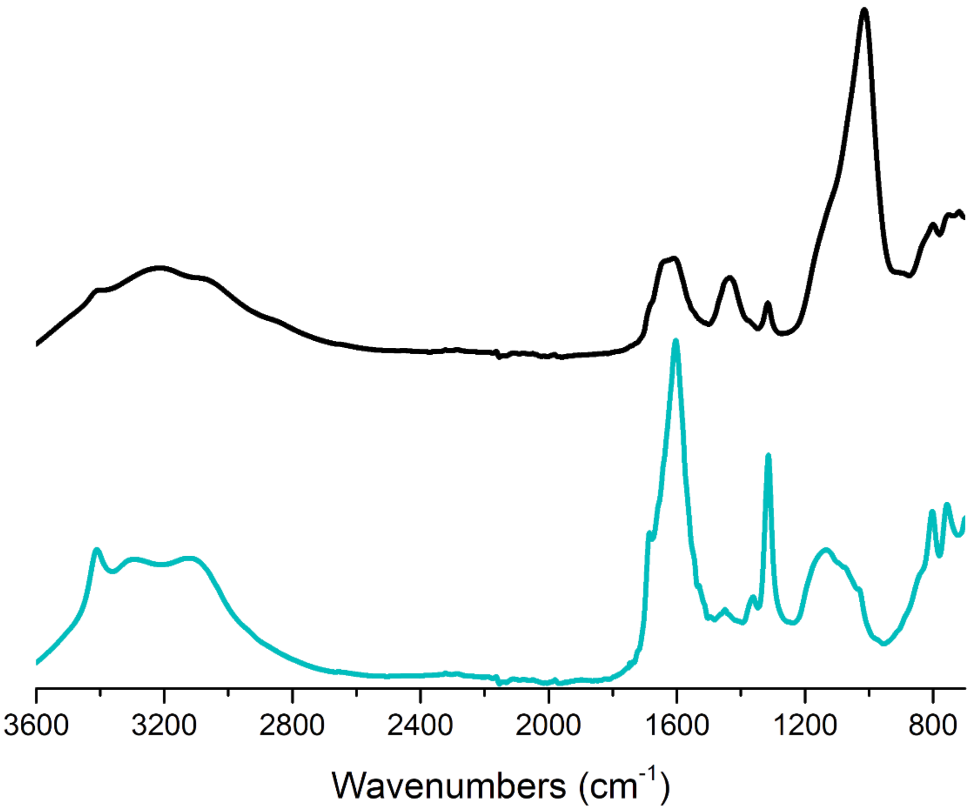

Figure S17 FTIR spectra of the white precipitate formed during oxidation of styrene catalyzed by **1** with $Sc(OTf)_3$ (2 eq.) in acetonitrile (black) or deuterated acetonitrile (cyan).

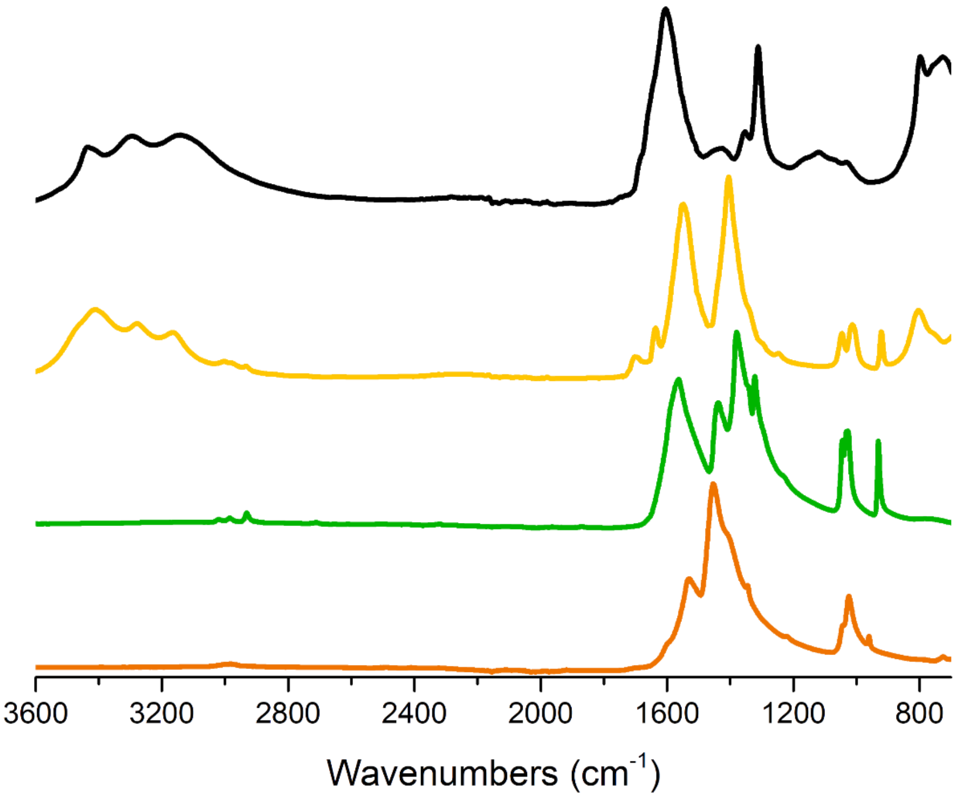

Figure S18 FTIR spectra of the white precipitate formed during oxidation of styrene catalyzed by **1** with $Sc(OTf)_3$ (2 eq.) in acetonitrile (black) compared to Na(OAc) (yellow), $Mn(OAc)_2$ (green), and $Sc(OAc)_3{\cdot}xH_2O$ (orange).

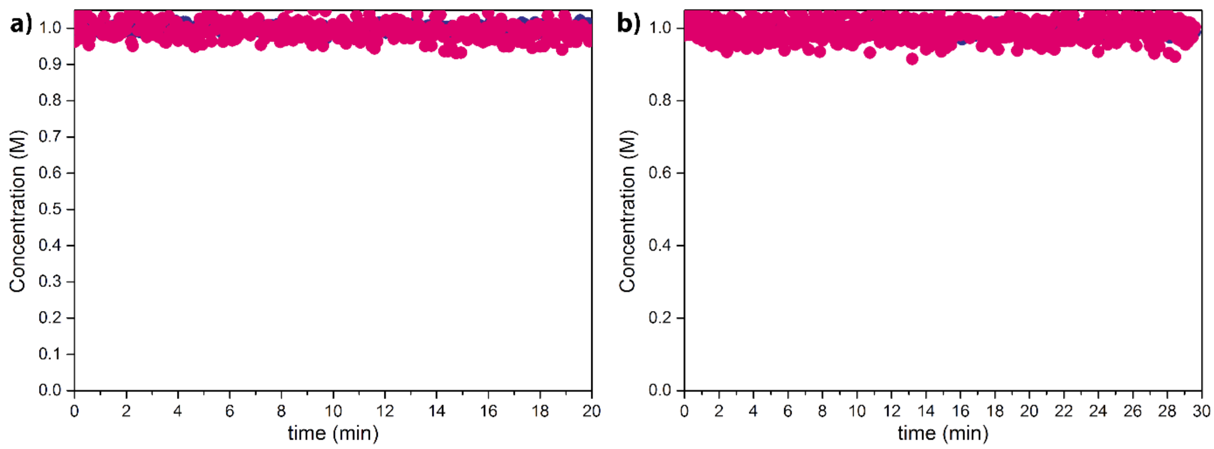

Figure S19 No styrene conversion (blue) nor H_2O_2 consumption (magenta) by a solution of (a) $Sc(OTf)_3$ (2 mM) or (b) tmtacn (1 mM) with $Sc(OTf)_3$ (2 mM) in CH_3CN.

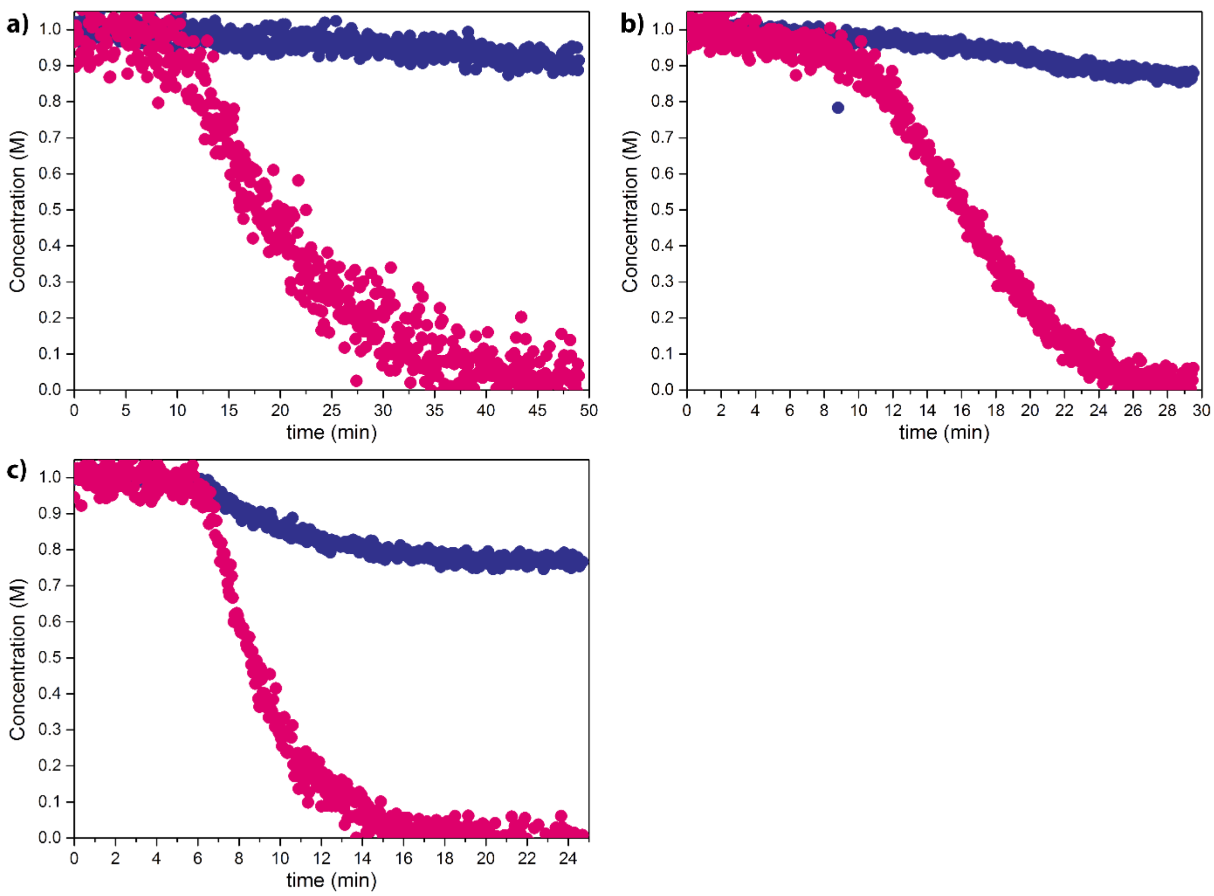

Figure S20 Consumption of H_2O_2 (magenta) and conversion of styrene (blue) by **1** (1 mM) activated by either (a) $Sc(OTf)_3$ (2 mM) with a 35 s standing time, (b) $Sc(OTf)_3$ (2 mM) with a 10 min standing time, or (c) $Al(OTf)_3$ (2 mM) with a 10 min standing time.

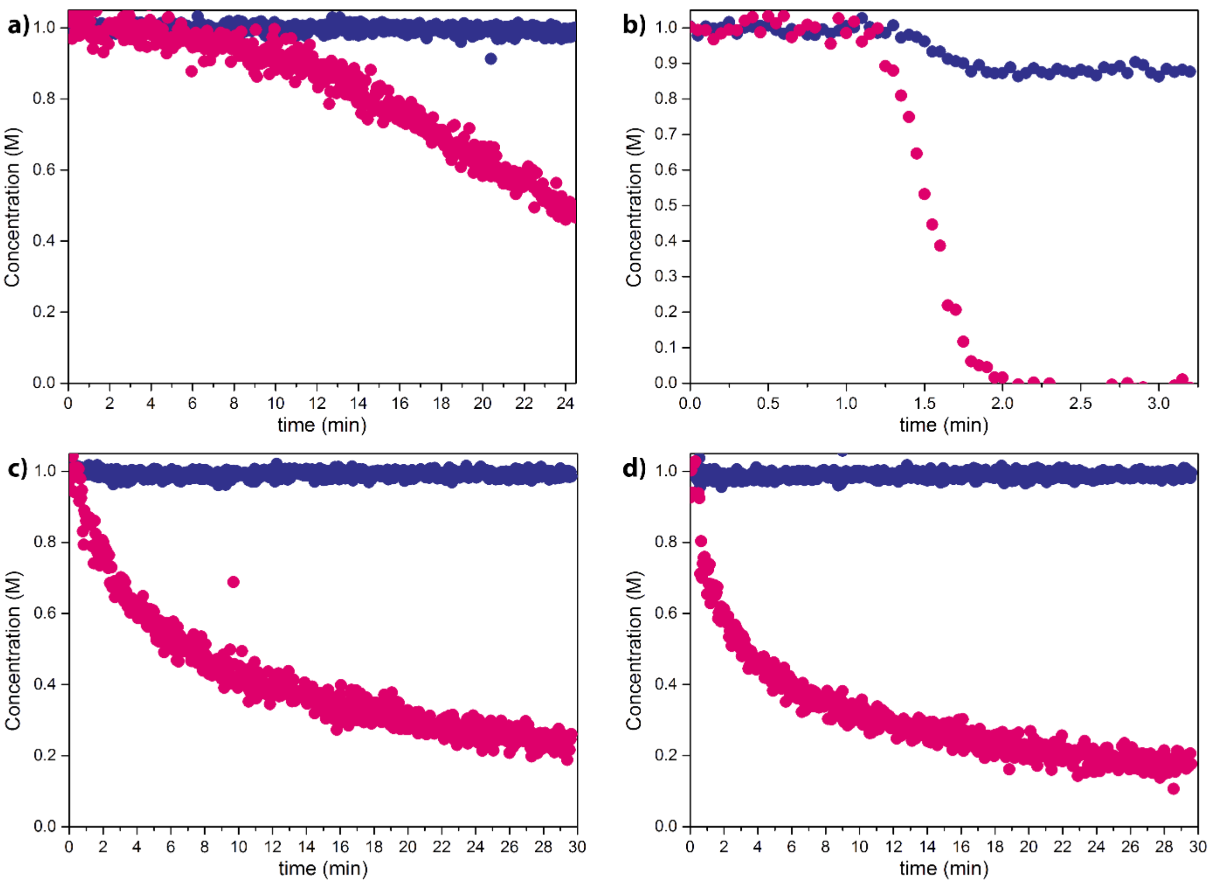

Figure S21 Comparison of kinetics of styrene conversion (blue) and H_2O_2 consumption (magenta) by **1** (1 mM) activated by either (a) $Y(OTF)_3$ (2 mM) with a 10 min standing time, (b) $Y(CF_3CO_2)_3$ (2 mM) with a 10 min standing time, (c) NaOTf (6 mM) with a 10 min standing time, or (d) NaOTf (6 mM) with a 17 h standing time.

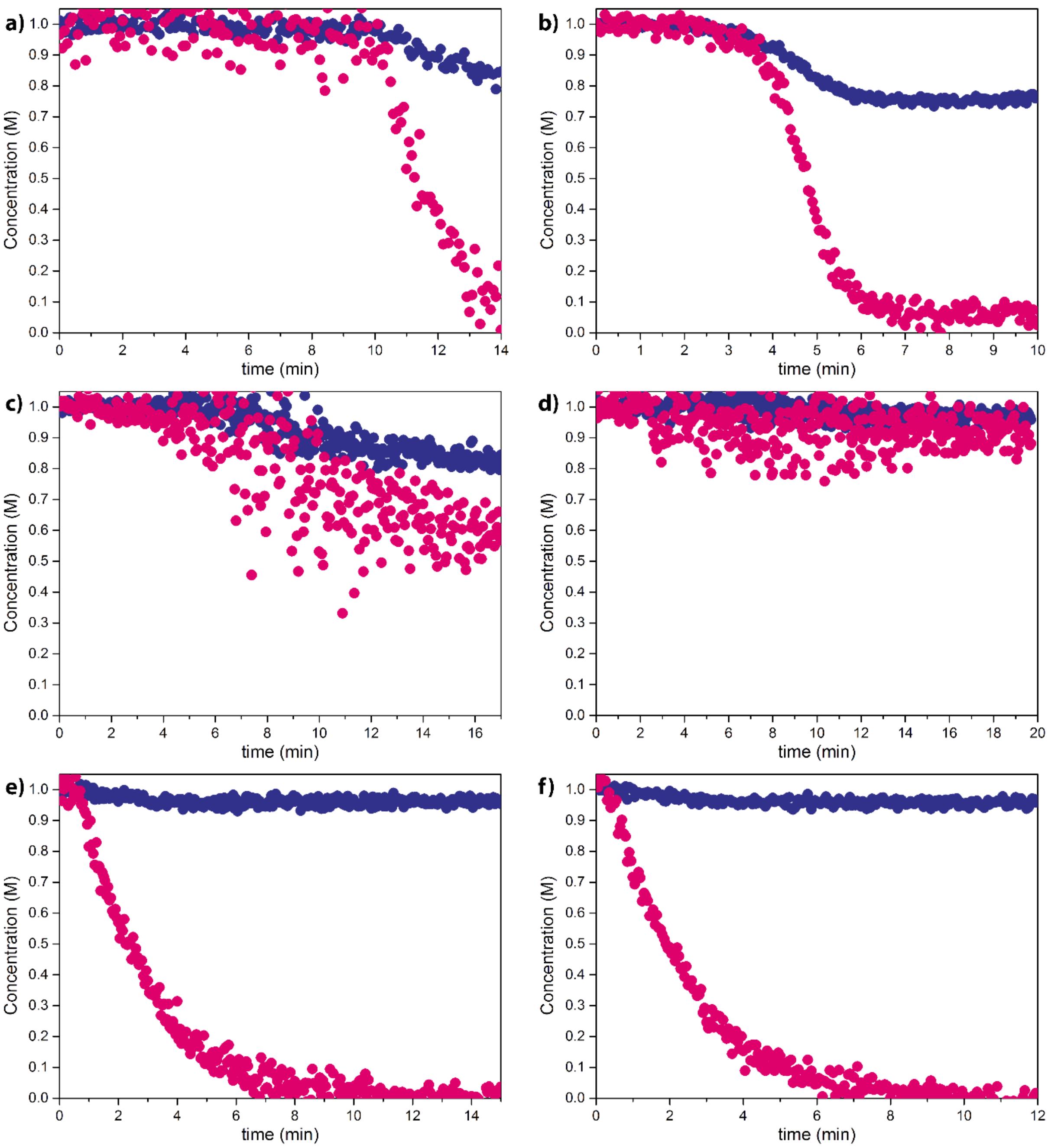

Figure S22 Comparison of kinetics of styrene conversion (blue) and H_2O_2 consumption (magenta) by **1** (1 mM) activated by either (a) TfOH (6 mM) with a 35 s standing time, (b) CF_3CO_2H (6 mM) with a 17 h standing time, (c) H_2SO_4 (6 mM) with a 10 min standing time, (d) H_2SO_4 (6 mM) with a 17 h standing time, (e) CH_3CO_2H (6 mM) with a 10 min standing time, or (f) CH_3CO_2H (6 mM) with a 17 h standing time.

Computational details

All Density Functional Theory (DFT) calculations were performed with the Amsterdam Density Functional (ADF) program (ADF 20016.01).[1,2] MOs were expanded in an uncontracted set of Slater type orbitals (STOs) of triple-zeta quality containing diffuse functions (TZ2P)[3] and two sets of polarization functions with all electrons treated explicitly. An auxiliary set of s, p, d, f, and g STOs were used to fit the molecular density and to represent the Coulomb and exchange potentials accurately for each SCF cycle.

Geometries were optimized until the maximum gradient component was less than 10^{-3} a.u. (default value is 10^{-3} a.u.). All calculations were performed using the BP86 Density Functional Approximation (DFA), proven to be good for structural data and thermodynamics.[4–6] For all calculations, the Becke grid[7,8] of good quality was used. COSMO[9–11] dielectric continuum model was used for implicit treatment of the environment (with methanol as a solvent).[12,13] Scalar relativistic corrections have been included self-consistently by using the zeroth-order regular approximation (ZORA).[14–16] Since calculations showed that manganese dimer is antiferromagnetically coupled S_A= 3/2 and S_B= 3/2 state, in order to obtain the geometry we have utilized broken-symmetry[17,18] (BS) calculations. Nature of stationary points were confirmed by calculating analytical Hessians, and the obtained Hessians have been further utilized for the isotopic shift calculations. In this approach, implemented in ADF program,[2]1 the rotations and translations are not projected out of the Hessian prior to the normal mode analysis and normal modes that belong to the original and the isotopically shifted frequencies are identified based on their overlap. We analyzed binding of H^+ and both neutral and positive Lewis acid(LA) fragment, i.e. $Ca(OTf)_2/Ca(OTf)^+$, $Zn(OTf)_2/Zn(OTf)^+$ and $Sc(OTf)_3/Sc(OTf)_2^+$ in order to attempt to treat all microscopic possibilities for catalytic activation.

The interaction of Sc (and other Lewis acids, Ca^{2+}, Zn^{2+}) and H^+ with $[Mn_2(\mu\text{-}O)_3(TMTACN)_2]^{2+}$

Binding of H^+ and both neutral and positive Lewis acid(LA) fragments, i.e. $Ca(OTf)_2/Ca(OTf)^+$, $Zn(OTf)_2/Zn(OTf)^+$ and $Sc(OTf)_3/Sc(OTf)_2^+$ were examined to treat all microscopic possibilities for catalytic activation. Table S1 shows that the most pronounced effect on the structure can be observed with scandium LA fragments. Table S2 indicates a substantial effect of the LAs on the redox properties of the complex. Although LA coordination reduces both the HOMO and LUMO energies, the effect on LUMO properties and energetics is most relevant. Binding of the Lewis acid lowers the energy of the LUMO orbitals (Table 2) with H^+ and Sc^{3+} showing the most pronounced effect. Furthermore, although Mn-O dissociation is not observed, there are significant distortions and bond elongations, most pronounced by the Sc based LAs. The interaction of the Lewis acid with **1** is, as expected, mostly ionic (which is inferred by the contribution of LAs to the dimer MOs), however, the covalent contribution is increasing in the following order: $Ca^{2+} < Zn^{2+} < Sc^{3+} < H^+$, and it is non negligible except for Ca^{2+}.

Table S1. Mn-Mn and Mn-O bond lengths in initial complex and after coordination of appropriate LA.

		Mn-Mn	**Mn-O**	**Mn-O**	**Mn-O**-LA
Initial complex	$[Mn_2(\mu\text{-}O)_3(TMTACN)_2]^{2+}$	2.22	1.79	1.79	1.79
Additive	H^+	2.28	1.78	1.78	1.94
	$Ca(OTf)_2$	2.32	1.82	1.82	1.91
	$Ca(OTf)^+$	2.33	1.82	1.83	1.92
	$Zn(OTf)_2$	2.35	1.82	1.82	1.93
	$Zn(OTf)^+$	2.38	1.82	1.82	1.95
	$Sc(OTf)_3$	2.39	1.82	1.82	2.02
	$Sc(OTf)_2^+$	2.40	1.82	1.82	2.02

Table S2. HOMO and LUMO energies and the contribution of the appropriate LA.

		HOMO	%LA	LUMO	%LA
Initial complex	$[Mn_2(\mu\text{-}O)_3(TMTACN)_2]^{2+}$	-5.625	-	-4.796	-
Additive	H^+	-6.948	-	-6.411	-
	$Ca(OTf)_2$	-7.341	-	-5.038	-
	$Ca(OTf)^+$	-7.530	-	-5.222	-
	$Zn(OTf)_2$	-7.443	-	-5.189	1.08
	$Zn(OTf)^+$	-7.761	-	-5.555	2.36
	$Sc(OTf)_3$	-7.830	-	-5.689	2.41
	$Sc(OTf)_2^+$	-8.063	-	-6.027	7.03

Calculation of ^{2}H and ^{18}O isotopic shift

Table S3. Frequency shifts produced by the isotope labelling for ($[Mn_2(\mu\text{-}O)_2(\mu\text{-}O^2H)(TMTACN)_2]^{2+}$)

Isotopic (^{2}H) Shift calculation				
Atom	Orig. Freq	Shifted Freq	shift	overlap
17	170.4	166.6	-3.8	1
28	252.4	249.7	-2.6	1
31	267.8	266.3	-1.6	0.9
35	293.2	289.2	-4	0.9
37	320.8	308.5	-12.2	0.8
38	320.8	318.1	-2.7	1
39	326.2	325	-1.1	0.9
42	339.6	335.9	-3.8	0.9
43	347.8	343.3	-4.5	1
60	518.5	512.7	-5.9	1
61	528.3	523.8	-4.5	1
62	561	562.8	1.9	0.9
68	661.4	662.5	1.1	1
70	710	551.3	-158.7	0.7
74	724.5	722.1	-2.4	0.9
77	792.7	594.5	-198.3	0.9
216	3604.6	2623.3	-981.4	1

Full listing showing unchanged bands also.

Isotopic (^{2}H) Shift calculation				
Atom	Orig. Freq	Shifted Freq	shift	overlap
1	-20.3	-20.3	0.0	1.0
2	-17.2	-17.2	0.0	1.0
3	-15.5	-15.5	0.0	1.0
4	-0.8	-0.8	0.0	1.0
5	0.0	0.0	0.0	1.0
6	0.8	0.8	0.0	1.0
7	15.3	15.3	0.0	1.0
8	65.8	65.8	-0.1	1.0
9	81.2	81.2	-0.1	1.0
10	94.7	94.7	0.0	1.0
11	97.6	97.5	-0.1	1.0
12	131.7	131.7	0.0	1.0
13	148.6	147.9	-0.7	1.0
14	152.8	152.7	-0.1	1.0
15	153.4	153.3	-0.1	1.0
16	158.8	158.7	0.0	1.0
17	170.4	166.6	-3.8	1.0
18	196.5	196.5	0.0	1.0
19	208.4	208.4	0.0	1.0
20	211.1	211.0	0.0	1.0
21	212.5	212.4	0.0	1.0
22	212.5	212.5	0.0	1.0
23	231.5	231.4	0.0	1.0
24	236.9	236.7	-0.2	1.0
25	246.6	246.2	-0.3	1.0
26	247.2	247.2	0.0	1.0
27	251.5	250.6	-0.9	1.0
28	252.4	249.7	-2.6	1.0
29	264.8	264.3	-0.5	0.9

30	267.0	267.0	0.0	1.0
31	267.8	266.3	-1.6	0.9
32	274.0	273.9	-0.2	1.0
33	275.4	275.2	-0.3	1.0
34	280.5	280.5	0.0	1.0
35	293.2	289.2	-4.0	0.9
36	300.9	300.6	-0.3	1.0
37	320.8	308.5	-12.2	0.8
38	320.8	318.1	-2.7	1.0
39	326.2	325.0	-1.1	0.9
40	328.7	328.1	-0.6	0.9
41	328.8	328.1	-0.7	0.9
42	339.6	335.9	-3.8	0.9
43	347.8	343.3	-4.5	1.0
44	367.5	367.2	-0.3	1.0
45	398.0	398.0	0.0	1.0
46	401.3	401.3	-0.1	1.0
47	402.7	402.1	-0.5	1.0
48	404.1	404.1	0.0	1.0
49	408.0	407.9	-0.1	1.0
50	409.1	409.0	-0.1	1.0
51	437.0	437.0	0.0	1.0
52	438.6	438.1	-0.6	1.0
53	444.8	444.8	-0.1	1.0
54	447.7	447.5	-0.1	1.0
55	448.3	448.3	0.0	1.0
56	451.1	451.1	0.0	1.0
57	453.1	453.1	-0.1	1.0
58	486.6	486.5	0.0	1.0
59	496.0	496.0	0.0	1.0
60	518.5	512.7	-5.9	1.0
61	528.3	523.8	-4.5	1.0
62	561.0	562.8	1.9	0.9
63	561.9	561.6	-0.3	1.0
64	564.8	564.8	0.0	1.0
65	569.9	569.9	0.0	1.0
66	585.4	585.5	0.2	1.0
67	585.7	585.7	0.0	1.0

68	661.4	662.5	1.1	1.0
69	691.1	691.8	0.7	1.0
70	710.0	551.3	-158.7	0.7
71	718.8	719.1	0.3	1.0
72	720.2	720.3	0.1	1.0
73	721.1	721.0	-0.1	0.9
74	724.5	722.1	-2.4	0.9
75	769.0	769.1	0.1	1.0
76	773.3	773.2	-0.1	1.0
77	792.7	594.5	-198.3	0.9
78	835.9	835.7	-0.3	1.0
79	836.4	836.4	0.0	1.0
80	872.8	872.8	0.0	1.0
81	874.6	874.6	0.0	1.0
82	875.9	875.8	0.0	1.0
83	877.2	877.2	0.0	1.0
84	943.8	943.8	0.0	1.0
85	945.5	945.4	-0.1	1.0
86	945.6	945.6	0.0	1.0
87	946.9	946.9	0.0	1.0
88	949.9	949.8	-0.1	1.0
89	950.8	950.8	0.0	1.0
90	972.6	972.6	0.0	1.0
91	973.5	973.5	0.0	1.0
92	975.2	975.2	0.0	1.0
93	976.6	976.6	0.0	1.0
94	980.0	980.0	0.0	1.0
95	981.4	981.4	0.0	1.0
96	1023.5	1023.5	0.0	1.0
97	1024.7	1024.7	0.0	1.0
98	1025.7	1025.7	0.0	1.0
99	1026.1	1026.1	0.0	1.0
100	1026.4	1026.4	0.0	1.0
101	1028.6	1028.6	0.0	1.0
102	1033.8	1033.8	0.0	1.0
103	1034.8	1034.8	0.0	1.0
104	1090.5	1090.5	0.0	1.0
105	1094.8	1094.8	0.0	1.0

106	1095.1	1095.1	0.0	1.0
107	1100.4	1100.4	0.0	1.0
108	1107.2	1107.2	0.0	1.0
109	1111.2	1111.2	0.0	1.0
110	1130.7	1130.7	0.0	1.0
111	1132.1	1132.1	0.0	1.0
112	1132.6	1132.6	0.0	1.0
113	1133.4	1133.4	0.0	1.0
114	1170.5	1170.5	0.0	1.0
115	1173.8	1173.8	0.0	1.0
116	1175.5	1175.5	0.0	1.0
117	1178.8	1178.8	0.0	1.0
118	1189.1	1189.1	0.0	1.0
119	1197.0	1197.0	0.0	1.0
120	1236.1	1236.1	0.0	1.0
121	1236.6	1236.6	0.0	1.0
122	1238.0	1238.0	0.0	1.0
123	1238.5	1238.5	0.0	1.0
124	1256.7	1256.7	0.0	1.0
125	1256.9	1256.9	0.0	1.0
126	1271.5	1271.5	0.0	1.0
127	1271.9	1271.9	0.0	1.0
128	1272.5	1272.5	0.0	1.0
129	1273.0	1273.0	0.0	1.0
130	1273.1	1273.1	0.0	1.0
131	1274.1	1274.1	0.0	1.0
132	1324.3	1324.3	0.0	1.0
133	1324.8	1324.7	0.0	1.0
134	1337.6	1337.6	0.0	1.0
135	1337.8	1337.8	0.0	1.0
136	1338.2	1338.2	0.0	1.0
137	1338.4	1338.4	0.0	1.0
138	1356.8	1356.8	0.0	1.0
139	1359.2	1359.2	0.0	1.0
140	1367.4	1367.4	0.0	1.0
141	1368.1	1368.1	0.0	1.0
142	1368.4	1368.4	0.0	1.0
143	1369.2	1369.2	0.0	1.0
144	1394.3	1394.1	-0.1	1.0
145	1397.6	1397.6	0.0	1.0
146	1398.1	1398.1	0.0	1.0
147	1401.5	1401.5	0.0	1.0
148	1402.6	1402.6	0.0	1.0
149	1404.3	1404.3	0.0	1.0
150	1422.6	1422.6	0.0	1.0
151	1427.4	1427.4	0.0	1.0
152	1427.7	1427.7	0.0	1.0
153	1430.4	1430.4	0.0	1.0
154	1430.8	1430.7	0.0	1.0
155	1431.4	1431.4	0.0	1.0
156	1432.4	1432.4	0.0	1.0
157	1434.0	1434.0	0.0	1.0
158	1434.2	1434.2	-0.1	1.0
159	1434.7	1434.7	0.0	1.0
160	1435.5	1435.5	0.0	1.0
161	1436.6	1436.6	0.0	1.0
162	1439.2	1439.1	0.0	1.0
163	1439.9	1439.9	0.0	1.0
164	1441.4	1441.3	0.0	1.0
165	1443.0	1443.0	0.0	1.0
166	1443.2	1443.2	0.0	1.0
167	1448.7	1447.9	-0.8	1.0
168	1449.2	1449.2	0.0	1.0
169	1456.9	1456.8	-0.1	1.0
170	1457.8	1457.7	-0.2	1.0
171	1465.3	1465.3	0.0	1.0
172	1470.8	1470.8	0.0	1.0
173	1471.5	1471.5	0.0	1.0
174	2973.9	2973.9	0.0	1.0
175	2975.2	2975.3	0.1	1.0
176	2979.1	2979.1	0.0	1.0
177	2979.8	2979.8	0.0	1.0
178	2983.9	2983.9	0.0	1.0
179	2985.4	2985.4	0.0	1.0
180	2985.5	2985.5	0.0	1.0
181	2985.7	2985.7	0.0	1.0

182	2986.4	2986.4	0.0	1.0
183	2986.5	2986.5	0.0	1.0
184	2990.6	2990.6	0.0	1.0
185	2990.8	2990.8	0.0	1.0
186	3017.0	3017.0	0.0	1.0
187	3017.1	3017.1	0.0	1.0
188	3019.1	3019.1	0.0	1.0
189	3019.3	3019.3	0.0	1.0
190	3023.7	3023.7	0.0	1.0
191	3024.0	3024.0	0.0	1.0
192	3039.6	3039.6	0.0	1.0
193	3039.6	3039.6	0.0	1.0
194	3043.6	3043.6	0.0	1.0
195	3043.7	3043.7	0.0	1.0
196	3046.9	3046.9	0.0	1.0
197	3047.0	3047.0	0.0	1.0
198	3047.2	3047.1	0.0	1.0
199	3048.1	3048.2	0.1	1.0
200	3067.4	3067.4	0.0	1.0
201	3067.5	3067.5	0.0	1.0
202	3068.3	3068.3	0.0	1.0
203	3069.8	3069.8	0.0	1.0
204	3070.0	3070.0	0.0	1.0
205	3070.2	3070.2	0.0	1.0
206	3072.8	3072.8	0.0	1.0
207	3076.6	3076.6	0.0	1.0
208	3077.5	3077.5	0.0	1.0
209	3077.6	3077.6	0.0	1.0
210	3090.6	3090.6	0.0	1.0
211	3093.8	3093.8	0.0	1.0
212	3102.4	3102.4	0.0	1.0
213	3103.8	3103.8	0.0	1.0
214	3114.7	3114.7	0.0	1.0
215	3121.3	3121.3	0.0	1.0
216	3604.6	2623.3	-981.4	1.0

Table S4. Frequency shifts produced by the isotope labelling for ([$Mn_2(\mu\text{-}O)_2(\mu\text{-}^{18}O)(TMTACN)_2]^{2+}$)

Isotopic (^2H) Shift calculation				
Atom	Orig. Freq	Shifted Freq	shift	overlap
17	177.5	167.9	-9.6	1
25	237.6	235.4	-2.2	0.9
26	237.9	235.7	-2.2	1
29	251.4	249.6	-1.7	1
32	272.7	269.9	-2.8	0.9
33	273.1	270.3	-2.8	0.8
42	388	373.7	-14.3	0.9
43	388.1	373.8	-14.3	0.9
47	406.2	403.6	-2.6	1
48	406.5	404	-2.5	1
49	412.3	394.6	-17.7	0.9
50	412.9	395	-17.8	0.9
60	507.8	488	-19.8	1
67	671.4	642.8	-28.5	1
68	671.8	643.3	-28.5	1
69	707	672.1	-34.9	1

Full listing showing unchanged bands also.

Isotopic (^2H) Shift calculation				
Atom	Orig. Freq	Shifted Freq	shift	overlap
1	-12.1	-12.1	0.0	1.0
2	-11.5	-11.4	0.0	1.0
3	-11.4	-11.3	0.0	1.0
4	0.0	0.0	0.0	1.0
5	0.7	0.7	0.0	1.0
6	2.7	2.7	0.0	1.0
7	30.7	30.7	0.0	1.0
8	76.7	76.4	-0.3	1.0
9	77.5	77.3	-0.3	1.0
10	99.0	98.9	-0.1	1.0
11	99.4	99.2	-0.1	1.0
12	133.2	133.2	0.0	1.0
13	153.6	153.1	-0.5	1.0
14	153.8	153.4	-0.5	1.0
15	157.9	157.8	-0.1	1.0
16	158.0	157.9	-0.1	1.0
17	177.5	167.9	-9.6	1.0
18	190.0	189.4	-0.6	1.0
19	210.1	209.6	-0.5	1.0
20	210.2	210.1	-0.1	1.0
21	210.4	209.9	-0.5	1.0
22	210.5	210.4	-0.1	1.0
23	226.9	226.9	0.0	1.0
24	237.5	237.4	-0.1	0.9
25	237.6	235.4	-2.2	0.9
26	237.9	235.7	-2.2	1.0
27	238.5	238.4	-0.1	1.0
28	241.8	241.7	-0.1	1.0
29	251.4	249.6	-1.7	1.0

30	268.7	268.7	0.0	1.0
31	270.5	270.6	0.1	0.8
32	272.7	269.9	-2.8	0.9
33	273.1	270.3	-2.8	0.8
34	274.1	273.6	-0.5	1.0
35	276.0	275.5	-0.5	1.0
36	281.3	281.3	-0.1	1.0
37	328.3	327.5	-0.8	1.0
38	328.6	327.8	-0.8	1.0
39	328.8	328.0	-0.8	1.0
40	329.0	328.3	-0.7	1.0
41	363.4	362.2	-1.1	1.0
42	388.0	373.7	-14.3	0.9
43	388.1	373.8	-14.3	0.9
44	398.7	399.5	0.8	0.9
45	398.8	398.6	-0.2	1.0
46	399.2	399.9	0.7	0.9
47	406.2	403.6	-2.6	1.0
48	406.5	404.0	-2.5	1.0
49	412.3	394.6	-17.7	0.9
50	412.9	395.0	-17.8	0.9
51	417.1	416.5	-0.6	1.0
52	431.6	431.6	0.0	1.0
53	445.0	444.8	-0.2	1.0
54	445.2	445.1	-0.2	1.0
55	445.4	445.4	-0.1	1.0
56	445.7	445.6	-0.1	1.0
57	451.1	450.2	-0.9	1.0
58	478.7	477.6	-1.1	1.0
59	492.6	492.0	-0.6	1.0
60	507.8	488.0	-19.8	1.0
61	563.3	563.3	0.0	1.0
62	563.4	563.4	0.0	1.0
63	563.4	562.7	-0.7	1.0
64	563.6	562.9	-0.7	1.0
65	587.0	586.9	-0.1	0.9

66	587.0	587.0	0.0	0.9
67	671.4	642.8	-28.5	1.0
68	671.8	643.3	-28.5	1.0
69	707.0	672.1	-34.9	1.0
70	724.9	724.9	0.0	1.0
71	725.3	725.3	0.0	1.0
72	727.2	726.7	-0.6	1.0
73	727.6	727.0	-0.6	1.0
74	770.0	769.8	-0.2	1.0
75	775.9	775.6	-0.3	1.0
76	839.6	839.6	0.0	1.0
77	840.1	840.1	0.0	1.0
78	878.9	878.9	0.0	1.0
79	879.0	879.0	0.0	1.0
80	880.2	880.2	0.0	1.0
81	880.3	880.3	0.0	1.0
82	957.5	957.5	0.0	1.0
83	957.6	957.6	0.0	1.0
84	958.6	958.6	0.0	1.0
85	958.8	958.7	0.0	1.0
86	959.5	959.5	0.0	1.0
87	961.2	961.2	0.0	1.0
88	980.9	980.9	0.0	1.0
89	981.1	981.1	0.0	1.0
90	982.3	982.3	0.0	1.0
91	982.6	982.6	0.0	1.0
92	984.9	984.8	0.0	1.0
93	986.6	986.6	0.0	1.0
94	1029.1	1029.1	0.0	1.0
95	1029.7	1029.7	0.0	1.0
96	1029.9	1029.9	0.0	1.0
97	1030.4	1030.4	0.0	1.0
98	1030.6	1030.6	0.0	1.0
99	1032.6	1032.6	0.0	1.0
100	1040.6	1040.6	0.0	1.0
101	1041.0	1041.0	0.0	1.0

102	1097.9	1097.9	0.0	1.0
103	1097.9	1097.9	0.0	1.0
104	1102.1	1102.1	0.0	1.0
105	1102.2	1102.2	0.0	1.0
106	1110.7	1110.7	0.0	1.0
107	1113.9	1113.9	0.0	1.0
108	1134.9	1134.9	0.0	1.0
109	1135.0	1135.0	0.0	1.0
110	1136.2	1136.2	0.0	1.0
111	1136.3	1136.3	0.0	1.0
112	1179.2	1179.2	0.0	1.0
113	1179.4	1179.4	0.0	1.0
114	1183.2	1183.2	0.0	1.0
115	1183.5	1183.5	0.0	1.0
116	1196.6	1196.6	0.0	1.0
117	1203.5	1203.5	0.0	1.0
118	1239.1	1239.1	0.0	1.0
119	1239.4	1239.4	0.0	1.0
120	1239.5	1239.5	0.0	1.0
121	1239.8	1239.8	0.0	1.0
122	1260.6	1260.6	0.0	1.0
123	1260.8	1260.8	0.0	1.0
124	1272.6	1272.6	0.0	1.0
125	1273.6	1273.6	0.0	1.0
126	1273.8	1273.8	0.0	1.0
127	1273.9	1273.9	0.0	1.0
128	1275.4	1275.4	0.0	1.0
129	1275.5	1275.4	0.0	1.0
130	1324.7	1324.7	0.0	1.0
131	1325.0	1325.0	0.0	1.0
132	1339.9	1339.9	0.0	1.0
133	1340.0	1340.0	0.0	1.0
134	1340.5	1340.5	0.0	1.0
135	1340.7	1340.7	0.0	1.0
136	1356.1	1356.1	0.0	1.0
137	1358.1	1358.1	0.0	1.0

138	1366.2	1366.2	0.0	1.0
139	1366.4	1366.4	0.0	1.0
140	1366.8	1366.8	0.0	1.0
141	1367.0	1367.0	0.0	1.0
142	1397.2	1397.2	0.0	1.0
143	1400.0	1400.0	0.0	1.0
144	1400.3	1400.3	0.0	1.0
145	1400.4	1400.4	0.0	1.0
146	1403.4	1403.4	0.0	1.0
147	1403.5	1403.5	0.0	1.0
148	1425.2	1425.2	0.0	1.0
149	1425.3	1425.3	0.0	1.0
150	1426.5	1426.5	0.0	1.0
151	1428.6	1428.6	0.0	1.0
152	1428.7	1428.7	0.0	1.0
153	1430.8	1430.8	0.0	1.0
154	1433.6	1433.6	0.0	1.0
155	1433.8	1433.8	0.0	1.0
156	1435.1	1435.0	0.0	1.0
157	1435.3	1435.3	0.0	1.0
158	1435.9	1435.9	0.0	1.0
159	1436.2	1436.2	0.0	1.0
160	1436.4	1436.4	0.0	1.0
161	1439.4	1439.4	0.0	1.0
162	1439.7	1439.7	0.0	1.0
163	1439.9	1439.9	0.0	1.0
164	1440.5	1440.5	0.0	1.0
165	1440.6	1440.6	0.0	1.0
166	1440.8	1440.8	0.0	1.0
167	1459.4	1459.4	0.0	1.0
168	1459.9	1459.9	0.0	1.0
169	1460.8	1460.8	0.0	1.0
170	1471.6	1471.6	0.0	1.0
171	1472.1	1472.1	0.0	1.0
172	2964.7	2964.7	0.0	1.0
173	2964.8	2964.8	0.0	1.0

174	2964.8	2964.8	0.0	1.0
175	2965.4	2965.4	0.0	1.0
176	2965.5	2965.5	0.0	1.0
177	2965.8	2965.8	0.0	1.0
178	2968.1	2968.1	0.0	1.0
179	2968.2	2968.2	0.0	1.0
180	2968.2	2968.2	0.0	1.0
181	2968.2	2968.2	0.0	1.0
182	2969.1	2969.1	0.0	1.0
183	2970.1	2970.1	0.0	1.0
184	3003.7	3003.7	0.0	1.0
185	3003.8	3003.8	0.0	1.0
186	3003.9	3003.9	0.0	1.0
187	3003.9	3003.9	0.0	1.0
188	3007.5	3007.5	0.0	1.0
189	3008.0	3008.0	0.0	1.0
190	3032.5	3032.5	0.0	1.0
191	3032.6	3032.6	0.0	1.0
192	3033.0	3033.0	0.0	1.0
193	3033.1	3033.1	0.0	1.0
194	3033.1	3033.1	0.0	1.0

195	3033.2	3033.2	0.0	1.0
196	3053.8	3053.8	0.0	1.0
197	3053.9	3053.9	0.0	1.0
198	3054.1	3054.1	0.0	1.0
199	3054.1	3054.1	0.0	1.0
200	3059.2	3059.2	0.0	1.0
201	3059.5	3059.5	0.0	1.0
202	3059.6	3059.6	0.0	1.0
203	3061.4	3061.4	0.0	1.0
204	3061.8	3061.8	0.0	1.0
205	3061.8	3061.8	0.0	1.0
206	3062.1	3062.1	0.0	1.0
207	3062.4	3062.4	0.0	1.0
208	3096.6	3096.6	0.0	1.0
209	3096.8	3096.8	0.0	1.0
210	3097.0	3097.0	0.0	1.0
211	3099.1	3099.1	0.0	1.0
212	3099.2	3099.2	0.0	1.0
213	3099.5	3099.5	0.0	1.0

Table S5. Frequency shifts produced by the isotope labelling for $[Mn_2(\mu\text{-}^{18}O)_2(\mu\text{-}^{18}OH)(TMTACN)_2]^{2+}$

Isotopic (^2H) Shift calculation				
Atom	Orig. Freq	Shifted Freq	shift	overlap
17	170.4	162.2	-8.2	1
25	246.6	243.9	-2.7	1
27	251.5	248.7	-2.8	1
28	252.4	248.8	-3.5	1
31	267.8	266.3	-1.6	0.9
33	275.4	272.6	-2.8	1
35	293.2	290.4	-2.8	1
36	300.9	300	-1	1
37	320.8	314.7	-6.1	0.9
38	320.8	316.9	-4	1
39	326.2	324	-2.2	0.9
41	328.8	326.6	-2.2	0.9
42	339.6	336.3	-3.4	1
43	347.8	341.4	-6.4	1
44	367.5	356.3	-11.3	1
52	438.6	420.7	-18	0.9
55	448.3	447.2	-1.1	0.9
60	518.5	495.1	-23.5	0.7
61	528.3	507.6	-20.8	1
68	661.4	633.5	-27.9	1
69	691.1	660.2	-30.9	1
70	710	704.7	-5.3	1
74	724.5	723.3	-1.2	1
77	792.7	789.2	-3.5	1
216	3604.6	3593	-11.7	1

Full listing showing unchanged bands also.

Isotopic (^2H) Shift calculation				
Atom	Orig. Freq	Shifted Freq	shift	overlap
1	-20.3	-20.2	0.1	1.0
2	-17.2	-17.2	0.0	1.0
3	-15.5	-15.5	0.0	1.0
4	-0.8	-0.8	0.0	1.0
5	0.0	0.0	0.0	1.0
6	0.8	0.8	0.0	1.0
7	15.3	15.3	0.0	1.0
8	65.8	65.6	-0.2	1.0
9	81.2	80.9	-0.3	1.0
10	94.7	94.6	-0.1	1.0
11	97.6	97.5	-0.1	1.0
12	131.7	131.7	-0.1	1.0
13	148.6	147.8	-0.8	1.0
14	152.8	152.7	-0.1	1.0

15	153.4	152.9	-0.5	1.0
16	158.8	158.6	-0.1	1.0
17	170.4	162.2	-8.2	1.0
18	196.5	196.2	-0.3	1.0
19	208.4	208.3	0.0	1.0
20	211.1	210.5	-0.5	1.0
21	212.5	212.0	-0.4	1.0
22	212.5	212.3	-0.2	1.0
23	231.5	231.4	-0.1	1.0
24	236.9	236.6	-0.3	1.0
25	246.6	243.9	-2.7	1.0
26	247.2	247.2	-0.1	1.0
27	251.5	248.7	-2.8	1.0
28	252.4	248.8	-3.5	1.0
29	264.8	264.0	-0.9	0.9
30	267.0	266.9	-0.1	1.0
31	267.8	266.3	-1.6	0.9
32	274.0	273.5	-0.5	1.0
33	275.4	272.6	-2.8	1.0
34	280.5	280.4	-0.1	1.0
35	293.2	290.4	-2.8	1.0
36	300.9	300.0	-1.0	1.0
37	320.8	314.7	-6.1	0.9
38	320.8	316.9	-4.0	1.0
39	326.2	324.0	-2.2	0.9
40	328.7	327.9	-0.8	1.0
41	328.8	326.6	-2.2	0.9
42	339.6	336.3	-3.4	1.0
43	347.8	341.4	-6.4	1.0
44	367.5	356.3	-11.3	1.0
45	398.0	397.5	-0.5	1.0
46	401.3	400.8	-0.5	1.0
47	402.7	402.4	-0.2	1.0
48	404.1	404.0	-0.1	1.0
49	408.0	407.2	-0.8	0.9
50	409.1	408.4	-0.7	0.9

51	437.0	436.7	-0.3	1.0
52	438.6	420.7	-18.0	0.9
53	444.8	444.3	-0.5	1.0
54	447.7	447.6	-0.1	1.0
55	448.3	447.2	-1.1	0.9
56	451.1	450.7	-0.5	1.0
57	453.1	453.1	-0.1	1.0
58	486.6	486.0	-0.6	1.0
59	496.0	495.8	-0.2	0.7
60	518.5	495.1	-23.5	0.7
61	528.3	507.6	-20.8	1.0
62	561.0	560.2	-0.7	1.0
63	561.9	561.9	0.0	1.0
64	564.8	564.8	0.0	1.0
65	569.9	569.0	-0.9	1.0
66	585.4	585.2	-0.1	1.0
67	585.7	585.7	0.0	1.0
68	661.4	633.5	-27.9	1.0
69	691.1	660.2	-30.9	1.0
70	710.0	704.7	-5.3	1.0
71	718.8	718.7	0.0	1.0
72	720.2	720.2	0.0	1.0
73	721.1	720.7	-0.4	1.0
74	724.5	723.3	-1.2	1.0
75	769.0	768.9	-0.1	1.0
76	773.3	773.2	-0.1	1.0
77	792.7	789.2	-3.5	1.0
78	835.9	835.9	0.0	1.0
79	836.4	836.4	0.0	1.0
80	872.8	872.8	0.0	1.0
81	874.6	874.6	0.0	1.0
82	875.9	875.9	0.0	1.0
83	877.2	877.2	0.0	1.0
84	943.8	943.8	0.0	1.0
85	945.5	945.5	0.0	1.0
86	945.6	945.6	0.0	1.0

87	946.9	946.9	0.0	1.0
88	949.9	949.9	0.0	1.0
89	950.8	950.8	0.0	1.0
90	972.6	972.6	0.0	1.0
91	973.5	973.5	0.0	1.0
92	975.2	975.2	0.0	1.0
93	976.6	976.6	0.0	1.0
94	980.0	980.0	0.0	1.0
95	981.4	981.4	0.0	1.0
96	1023.5	1023.5	0.0	1.0
97	1024.7	1024.7	0.0	1.0
98	1025.7	1025.7	0.0	1.0
99	1026.1	1026.1	0.0	1.0
100	1026.4	1026.4	0.0	1.0
101	1028.6	1028.6	0.0	1.0
102	1033.8	1033.8	0.0	1.0
103	1034.8	1034.8	0.0	1.0
104	1090.5	1090.5	0.0	1.0
105	1094.8	1094.8	0.0	1.0
106	1095.1	1095.1	0.0	1.0
107	1100.4	1100.4	0.0	1.0
108	1107.2	1107.2	0.0	1.0
109	1111.2	1111.2	0.0	1.0
110	1130.7	1130.7	0.0	1.0
111	1132.1	1132.1	0.0	1.0
112	1132.6	1132.6	0.0	1.0
113	1133.4	1133.4	0.0	1.0
114	1170.5	1170.5	0.0	1.0
115	1173.8	1173.8	0.0	1.0
116	1175.5	1175.5	0.0	1.0
117	1178.8	1178.8	0.0	1.0
118	1189.1	1189.1	0.0	1.0
119	1197.0	1197.0	0.0	1.0
120	1236.1	1236.1	0.0	1.0
121	1236.6	1236.6	0.0	1.0
122	1238.0	1238.0	0.0	1.0

123	1238.5	1238.5	0.0	1.0
124	1256.7	1256.7	0.0	1.0
125	1256.9	1256.9	0.0	1.0
126	1271.5	1271.5	0.0	1.0
127	1271.9	1271.9	0.0	1.0
128	1272.5	1272.5	0.0	1.0
129	1273.0	1273.0	0.0	1.0
130	1273.1	1273.1	0.0	1.0
131	1274.1	1274.1	0.0	1.0
132	1324.3	1324.3	0.0	1.0
133	1324.8	1324.8	0.0	1.0
134	1337.6	1337.6	0.0	1.0
135	1337.8	1337.8	0.0	1.0
136	1338.2	1338.2	0.0	1.0
137	1338.4	1338.4	0.0	1.0
138	1356.8	1356.8	0.0	1.0
139	1359.2	1359.2	0.0	1.0
140	1367.4	1367.4	0.0	1.0
141	1368.1	1368.1	0.0	1.0
142	1368.4	1368.4	0.0	1.0
143	1369.2	1369.2	0.0	1.0
144	1394.3	1394.3	0.0	1.0
145	1397.6	1397.6	0.0	1.0
146	1398.1	1398.1	0.0	1.0
147	1401.5	1401.5	0.0	1.0
148	1402.6	1402.6	0.0	1.0
149	1404.3	1404.3	0.0	1.0
150	1422.6	1422.6	0.0	1.0
151	1427.4	1427.4	0.0	1.0
152	1427.7	1427.7	0.0	1.0
153	1430.4	1430.4	0.0	1.0
154	1430.8	1430.8	0.0	1.0
155	1431.4	1431.4	0.0	1.0
156	1432.4	1432.4	0.0	1.0
157	1434.0	1434.0	0.0	1.0
158	1434.2	1434.2	0.0	1.0

159	1434.7	1434.7	0.0	1.0
160	1435.5	1435.5	0.0	1.0
161	1436.6	1436.6	0.0	1.0
162	1439.2	1439.2	0.0	1.0
163	1439.9	1439.9	0.0	1.0
164	1441.4	1441.3	0.0	1.0
165	1443.0	1443.0	0.0	1.0
166	1443.2	1443.2	0.0	1.0
167	1448.7	1448.7	0.0	1.0
168	1449.2	1449.2	0.0	1.0
169	1456.9	1456.9	0.0	1.0
170	1457.8	1457.8	0.0	1.0
171	1465.3	1465.3	0.0	1.0
172	1470.8	1470.8	0.0	1.0
173	1471.5	1471.5	0.0	1.0
174	2973.9	2973.9	0.0	1.0
175	2975.2	2975.2	0.0	1.0
176	2979.1	2979.1	0.0	1.0
177	2979.8	2979.8	0.0	1.0
178	2983.9	2983.9	0.0	1.0
179	2985.4	2985.4	0.0	1.0
180	2985.5	2985.5	0.0	1.0
181	2985.7	2985.7	0.0	1.0
182	2986.4	2986.4	0.0	1.0
183	2986.5	2986.5	0.0	1.0
184	2990.6	2990.6	0.0	1.0
185	2990.8	2990.8	0.0	1.0
186	3017.0	3017.0	0.0	1.0
187	3017.1	3017.1	0.0	1.0
188	3019.1	3019.1	0.0	1.0
189	3019.3	3019.3	0.0	1.0
190	3023.7	3023.7	0.0	1.0
191	3024.0	3024.0	0.0	1.0
192	3039.6	3039.6	0.0	1.0
193	3039.6	3039.6	0.0	1.0
194	3043.6	3043.6	0.0	1.0
195	3043.7	3043.7	0.0	1.0
196	3046.9	3046.9	0.0	1.0
197	3047.0	3047.0	0.0	1.0
198	3047.2	3047.2	0.0	1.0
199	3048.1	3048.1	0.0	1.0
200	3067.4	3067.4	0.0	1.0
201	3067.5	3067.5	0.0	1.0
202	3068.3	3068.3	0.0	1.0
203	3069.8	3069.8	0.0	1.0
204	3070.0	3070.0	0.0	1.0
205	3070.2	3070.2	0.0	1.0
206	3072.8	3072.8	0.0	1.0
207	3076.6	3076.6	0.0	1.0
208	3077.5	3077.5	0.0	1.0
209	3077.6	3077.6	0.0	1.0
210	3090.6	3090.6	0.0	1.0
211	3093.8	3093.8	0.0	1.0
212	3102.4	3102.4	0.0	1.0
213	3103.8	3103.8	0.0	1.0
214	3114.7	3114.7	0.0	1.0
215	3121.3	3121.3	0.0	1.0
216	3604.6	3593.0	-11.7	1.0

References

(1) Baerends, E. J.; Autschbach, J.; Berces, A.; Bo, C.; Boerrigter, P. M.; Cavallo, L.; Chong, D. P.; Deng, L.; Dickson, R. M.; Ellis, D. E.; et al. ADF 20016.01. SCM: Amsterdam 2016.

(2) te Velde, G.; Bickelhaupt, F. M.; Baerends, E. J.; Fonseca Guerra, C.; van Gisbergen, S. J. A.; Snijders, J. G.; Ziegler, T. Chemistry with ADF. *J. Comput. Chem.* **2001**, *22* (9), 931–967.

(3) Van Lenthe, E.; Baerends, E. J. Optimized Slater-Type Basis Sets for the Elements 1–118. *J. Comput. Chem.* **2003**, *24* (9), 1142–1156. https://doi.org/10.1002/jcc.10255.

(4) Becke, A. D. Density-Functional Exchange-Energy Approximation with Correct Asymptotic Behavior. *Phys. Rev. A* **1988**, *38* (6), 3098–3100.

(5) Perdew, J. P. Density-Functional Approximation for the Correlation Energy of the Inhomogeneous Electron Gas. *Phys. Rev. B* **1986**, *33* (12), 8822–8824.

(6) Vlahovic, F. Z.; Gruden, M.; Stepanovic, S.; Swart, M. Density Functional Approximations for Consistent Spin and Oxidation States of Oxoiron Complexes. https://doi.org/10.26434/chemrxiv.8969741.

(7) Becke, A. D. A Multicenter Numerical Integration Scheme for Polyatomic Molecules. *J. Chem. Phys.* **1988**, *88* (4), 2547–2553. https://doi.org/doi:http://dx.doi.org/10.1063/1.454033.

(8) Franchini, M.; Philipsen, P. H. T.; Visscher, L. The Becke Fuzzy Cells Integration Scheme in the Amsterdam Density Functional Program Suite. *J. Comput. Chem.* **2013**, *34* (21), 1819–1827. https://doi.org/10.1002/jcc.23323.

(9) Klamt, A. Conductor-like Screening Model for Real Solvents: A New Approach to the Quantitative Calculation of Solvation Phenomena. *J. Phys. Chem.* **1995**, *99* (7), 2224–2235. https://doi.org/10.1021/j100007a062.

(10) Klamt, A.; Jonas, V. Treatment of the Outlying Charge in Continuum Solvation Models. *J. Chem. Phys.* **1996**, *105* (22), 9972–9981. https://doi.org/doi:http://dx.doi.org/10.1063/1.472829.

(11) Klamt, A.; Schuurmann, G. COSMO: A New Approach to Dielectric Screening in Solvents with Explicit Expressions for the Screening Energy and Its Gradient. *J. Chem. Soc. Perkin Trans. 2* **1993**, No. 5, 799–805. https://doi.org/10.1039/P29930000799.

(12) Pye, C. C.; Ziegler, T. An Implementation of the Conductor-like Screening Model of Solvation within the Amsterdam Density Functional Package. *Theor. Chem. Acc.* **1999**, *101* (6), 396–408. https://doi.org/10.1007/s002140050457.

(13) Swart, M.; Rösler, E.; Bickelhaupt, F. M. Proton Affinities in Water of Maingroup-Element Hydrides – Effects of Hydration and Methyl Substitution. *Eur. J. Inorg. Chem.* **2007**, *2007* (23), 3646–3654. https://doi.org/10.1002/ejic.200700228.

(14) Lenthe, E. van; Baerends, E. J.; Snijders, J. G. Relativistic Regular Two-component Hamiltonians. *J. Chem. Phys.* **1993**, *99* (6), 4597–4610. https://doi.org/doi:http://dx.doi.org/10.1063/1.466059.

(15) van Lenthe, E.; Baerends, E. J.; Snijders, J. G. Relativistic Total Energy Using Regular Approximations. *J. Chem. Phys.* **1994**, *101* (11), 9783–9792. https://doi.org/doi:http://dx.doi.org/10.1063/1.467943.

(16) van Lenthe, E.; Ehlers, A.; Baerends, E.-J. Geometry Optimizations in the Zero Order Regular Approximation for Relativistic Effects. *J. Chem. Phys.* **1999**, *110* (18), 8943–8953. https://doi.org/doi:http://dx.doi.org/10.1063/1.478813.

(17) Noodleman, L. Valence Bond Description of Antiferromagnetic Coupling in Transition Metal Dimers. *J. Chem. Phys.* **1981**, *74* (10), 5737–5743. https://doi.org/10.1063/1.440939.

(18) Noodleman, L.; Baerends, E. J. Electronic Structure, Magnetic Properties, ESR, and Optical Spectra for 2-Iron Ferredoxin Models by LCAO-X.Alpha. Valence Bond Theory. *J. Am. Chem. Soc.* **1984**, *106* (8), 2316–2327. https://doi.org/10.1021/ja00320a017.